Molecular Neurobiology (2026) 63:796
https://doi.org/10.1007/s12035-026-06076-4

RESEARCH

Neuroprotective Effect of Chitosan Nanoparticle–Delivered Orientin Against Hypoxia-Induced Brain Injury in Rats

İhsan Topaloğlu[1] · Çağrı Atasoy[1] · Gülfem Özduygu[2] · Eren Erdoğdu[3] · Güntuğ Batıhan[4] · Volkan Gelen[5] · Ali Yeşildağ[6] · Adem Kara[7] · Elif Erbaş[8]

Received: 21 December 2025 / Accepted: 16 July 2026
© The Author(s), under exclusive licence to Springer Science+Business Media, LLC, part of Springer Nature 2026

Abstract

Reduced brain oxygenation rapidly amplifies oxidative and inflammatory injury, creating a self-perpetuating cascade that can end in neuronal loss. Orientin can activate Nrf2/ARE-dependent antioxidant responses and suppress NF-κB–mediated inflammation, but poor solubility and limited bioavailability weaken its therapeutic impact. Here, we used chitosan nanoparticles (CNPs) to improve Orientin delivery and evaluated the protective effects of CNPs/Orientin on oxidative stress, inflammation, and apoptosis in hypoxia-induced brain injury. Forty-eight male Wistar albino rats were split into eight groups: (Control, Orientin, CNPs, CNPs/Orientin, Hypoxia, Hypoxia+Orientin, Hypoxia+CNPs, Hypoxia+CNPs/Orientin). The hypoxia model was applied with an 8% O_2+92% N_2 gas mixture for 8 h per day for 7 days. Orientin (40 mg/kg/day, i.p.) was administered simultaneously with the hypoxia period. MDA, SOD, GSH, BDNF, HIF-1α, iNOS, IL-1β, and TNF-α levels were determined by ELISA; gene expressions of Caspase-3, Bcl-2, HO-1, NRF2, NF-κB, and TNF-α were quantified by RT-PCR. Histological evaluations were performed in the cortex and hippocampus regions. CNPs/Orientin had a mean diameter of ~245 nm, a positive zeta potential (+29 mV), 81.3% encapsulation efficiency, and sustained release (79.6% over 72 h). Hypoxia significantly decreased SOD, GSH, and BDNF, while increasing MDA, HIF-1α, iNOS, and Caspase-3 levels ($p < 0.05$). All treatment groups attenuated the hypoxia-induced increase in IL-1β and TNF-α; however, cytokine levels did not differ significantly among the treatment arms. In the Hypoxia+CNPs/Orientin group, oxidative/nitrosative markers and neuronal histopathological findings were improved compared with hypoxia. Orientin delivered via chitosan nanoparticles demonstrated a significant neuroprotective effect, reducing oxidative stress, inflammation, and apoptosis while preserving neuronal structural integrity in hypoxia-induced brain injury. These results suggest that the nano-carrier form of Orientin may be a potential therapeutic agent in neurodegenerative processes.

Keywords Orientin · Chitosan nanoparticle · Hypoxia · Oxidative stress · Inflammation · Neuroprotection

✉ İhsan Topaloğlu
ras-topal@hotmail.com

[1] Department of Pulmonology, Kafkas University Faculty of Medicine, Kars, Turkey

[2] Department of Pulmonology, University of Health Science, Yedikule Chest Diseases and Thoracic Surgery Training and Research Hospital, Istanbul, Turkey

[3] Department of Thoracic Surgery, Istanbul University Faculty of Medicine, Istanbul, Turkey

[4] Department of Thoracic Surgery, Kafkas University Faculty of Medicine, Kars, Turkey

[5] Department of Physiology, Veterinary Faculty, Kafkas University, Kars, Turkey

[6] Faculty of Engineering and Architecture, Department of Bioengineering, Kafkas University, Kars, Turkey

[7] Department of Genetics, Faculty of Science, Erzurum Technical University, Erzurum, Turkey

[8] Department of Histology and Embryology, Faculty of Veterinary Medicine, Atatürk University, Erzurum, Turkey

Published online: 29 July 2026

Introduction

Hypoxia-induced brain injury is a complex neuropathological process characterized by oxidative stress, inflammation, and cellular energy dysfunction resulting from a decrease in oxygen supply. Increased reactive oxygen species (ROS) under hypoxic conditions accelerate lipid peroxidation while suppressing antioxidant systems such as superoxide dismutase (SOD) and glutathione (GSH) [1]. This redox imbalance, combined with an increase in cytokines such as interleukin-1β (IL-1β) and tumor necrosis factor-α (TNF-α), leads to impaired neuronal integrity and vascular permeability [2].

Hypoxia-activated hypoxia-inducible factor-1 alpha (HIF-1α) deepens nitrosative stress by increasing the expression of inducible nitric oxide synthase (iNOS). Concordantly, the reduction in brain-derived neurotrophic factor (BDNF) levels impairs synaptic plasticity and neuronal repair capacity [3–5]. These molecular disruptions result histologically in neuronal vacuolization, perivascular expansion, and hippocampal neuronal loss [6]. This multi-layered picture demonstrates that hypoxic brain injury progresses not only at the oxidative stress level but also at the inflammatory and structural levels.

In the search for effective multi-target therapeutic strategies against hypoxia-induced brain injury, naturally occurring flavonoids have attracted increasing attention due to their ability to modulate oxidative stress, inflammation, and cell survival pathways [7, 8]. Orientin is a naturally occurring flavonoid with well-documented antioxidant, anti-inflammatory, and neuroprotective properties, and previous studies have demonstrated that it exerts these effects primarily through activation of the Nrf2/ARE signaling pathway and suppression of NF-κB–mediated inflammation, both of which play critical roles in hypoxia-induced brain injury [9, 10]. However, the therapeutic application of orientin is limited by its poor solubility and low bioavailability. To overcome these limitations, chitosan nanoparticles (CNPs) were selected as a delivery system because of their biodegradable and biocompatible structure, ability to enhance tissue penetration, and immunomodulatory properties [11]. Accordingly, the present study aimed to evaluate the combined effects of orientin and CNPs on oxidative stress, inflammatory response, neurotrophic signaling, and histological integrity in a rat model of hypoxia-induced brain injury.

Materials and Methods

Synthesis and Characterization of CNPs and CNPs/Orientin

In this study, for the synthesis of CNPs, commercially obtained chitosan (Sigma, 448869) was first prepared at a concentration of 1 mg/mL in 1% acetic acid using a magnetic stirrer, and the mixture was stirred at 25 °C until a homogeneous solution was formed. Next, the pH of the solution was adjusted to 5.0 with 1 M sodium hydroxide (NaOH) solution. In the subsequent step, 20 mL of 0.04 M sodium citrate ($Na_3C_6H_5O_7$) was added to this mixture and stirred until a yellow color, indicating the formation of CNPs, was observed. The obtained CNPs were dried in an oven at 95 °C for approximately 24 h and preserved in the dark, ready for use [12, 13].

In this study, to obtain the CNPs/orientin structure, the orientin was first mixed with the chitosan nanoparticles we synthesized for approximately 4–5 h in a magnetic stirrer. CNPs and orientin interacted electrostatically to form CNPs/orientin structures. The encapsulation efficiency (EE) and drug loading (DL) of orientin-loaded chitosan nanoparticles (CNPs/Orientin) were determined indirectly by measuring the amount of free (non-encapsulated) orientin remaining in the supernatant after nanoparticle preparation. Briefly, the nanoparticle suspension was centrifuged at 15,000 × g for 30 min at 4 °C. The supernatant containing the unencapsulated orientin was carefully collected, and the concentration of free orientin was quantified using a UV–Vis spectrophotometer at the maximum absorption wavelength of orientin ($\lambda = 325$ nm) against an appropriate calibration curve. The encapsulation efficiency (EE) and drug loading (DL) were calculated using the following equations:

$$EE(\%) = [(Wt - Wf)/Wt] \times 100 \quad (1)$$

$$DL(\%) = [(Wt - Wf)/WNP] \times 100 \quad (2)$$

where

- Wt = total amount of orientin initially added during nanoparticle preparation (mg)
- Wf = amount of free (unencapsulated) orientin detected in the supernatant (mg)
- WNP = total weight of the recovered orientin-loaded nanoparticles (mg)

In Vitro Release Study

The in vitro release profile of orientin from chitosan nanoparticles was evaluated under physiological conditions

using the diffusion method. Briefly, chitosan nanoparticles loaded with a known amount of orientin were dispersed in phosphate-buffered saline (PBS, pH 7.4). They were then immersed in 50 mL of fresh PBS and incubated at 37 ± 0.5 °C under continuous agitation to simulate physiological conditions. At predetermined time intervals (0.5, 1, 3, 12, 24, 48, and 72 h), 2 mL of the release medium was withdrawn and replaced with an equal volume of fresh PBS to maintain sink conditions. The amount of released orientin was quantified spectrophotometrically at its maximum absorption wavelength ($\lambda = 325$ nm) using a UV–Vis spectrophotometer [14, 15]. The cumulative percentage of drug release was calculated based on a previously prepared calibration curve of orientin. All experiments were performed in triplicate ($n = 3$), and results are expressed as mean ± standard deviation (SD).

To confirm the formation of CNPs and CNPs/orientin structures, a Multiskan Sky, a Thermo Scientific brand, ultraviolet–visible (UV–Vis) spectrometer operating in the 200–900 nm range was used. To determine the functional groups in the characterization of CNPs, Fourier transform infrared spectroscopy (FT-IR) using a Perkin Elmer-Tensor 27 operating in the 400–4000 cm^{-1} wavelength range was employed. Particle size, polydispersity index (PDI), and zeta potential measurements were carried out using a Zetasizer Nano ZSP (Malvern Panalytical, Worcestershire, UK). Nanoparticles were dispersed in ultrapure water and sonicated for 10 min prior to analysis. Measurements were conducted in triplicate at 25 °C. The size and morphology of the CNPs were characterized using a scanning electron microscope (SEM) (FEI QUANTA model FEG 450). In addition, both size and morphology characterization of the CNPs were performed using a transmission electron microscope (TEM) (Hitachi model HighTech-7700).

Experimental Animals and Groups

A total of 48 male Wistar albino rats (220–250 g, 8–10 weeks old, $n = 6$ per group) were used in the study. The rats were obtained from the Kafkas University Experimental Animal Application and Research Center and housed under standard laboratory conditions (22 ± 2 °C, 55 ± 10% relative humidity, 12-h light/12-h dark cycle). All rats had free access to water and standard pellet food. The experimental protocol was approved by the Kafkas University Local Ethics Committee for Animal Experiments (Ethical Approval No: KAU-HADYEK-KAÜ-HADYEK/2025/245). The number of animals per group was determined based on previous experimental hypoxia studies reporting statistically significant differences in biochemical, molecular, and histopathological parameters with similar sample sizes, while also adhering to ethical principles aimed at minimizing animal use. The rats were divided into eight groups ($n = 6$) using a computer-assisted randomization method:

Control group: Rats kept under normoxic conditions without any intervention.
Orientin group: Rats administered Orientin under normoxic conditions.
CNPs group: Rats administered chitosan nanoparticles (CNPs) under normoxic conditions.
CNPs/Orientin group: Rats treated only with the combination (orientin-loaded CNPs) under normoxic conditions.
Hypoxia group: Rats exposed to hypoxia (8% O_2 + 92% N_2) for 8 h/day for 7 days.
Hypoxia+Orientin group: Rats administered orientin in addition to hypoxia.
Hypoxia+CNPs group: Rats administered CNPs in addition to hypoxia.
Hypoxia+CNPs/Orientin group: Rats exposed to hypoxia and treated with orientin-loaded CNPs.

The rats were monitored daily throughout the study, and mortality was not observed.

Hypoxia Model

The hypoxia protocol was adapted from previously described controlled/normobaric hypoxia approaches in rats with minor modifications [16]. Rats assigned to the hypoxia groups were exposed to a premixed hypoxic gas (8% O_2, 92% N_2) for 8 h/day over 7 consecutive days in a sealed, custom-built hypoxia chamber. The chamber was constructed from 1-cm-thick transparent polypropylene, and gas-tightness at all junctions was ensured using triple-layer silicone gaskets. The system was equipped with 8″ neoprene glove ports to allow in-chamber handling, a mixed-gas regulator, an inlet line, and an exhaust/outlet line to maintain continuous flow-through conditions.

Before each exposure, the chamber was pre-flushed (purged) with the premixed gas until the target oxygen concentration was reached. During each hypoxia session, the chamber O_2 concentration was continuously monitored using an integrated sensor and maintained at 8%. Temperature and humidity were monitored with digital sensors to ensure stable environmental conditions. To maintain steady hypoxia and minimize rebreathing/hypercapnia risk, the chamber was operated under continuous flow-through ventilation, with total gas flow scaled to animal load at approximately 2.5 L/min per rat. Premixed gas was supplied from high-pressure cylinders (150 bar) through a regulator system and was vented via the outlet line under controlled conditions. Throughout the hypoxia period, all

dosing and necessary manipulations were performed via the glove ports to minimize contact with normoxic ambient air.

Animals were exposed at a fixed time window each day and were observed throughout exposure for general condition (activity, respiratory pattern, agitation/lethargy, excessive salivation, etc.). Humane endpoints were predefined, and animals showing significant distress were to be removed from the protocol according to institutional guidelines.

The physiological effectiveness of hypoxia exposure was confirmed by arterial blood gas analysis in randomly selected rats. Mean post-exposure PaO_2 values were ~45–55 mmHg, which is consistent with experimental hypoxia models reported in the literature [17]. No acute distress or mortality was observed during the experimental period.

Treatment Protocol, Blood and Tissue Sampling, and Biochemical Analyses

During the intermittent hypoxia protocol, rats in the treatment groups received once-daily intraperitoneal injections for 7 consecutive days: orientin (40 mg/kg) [18]. chitosan nanoparticles (50 mg/kg) [19], or orientin-loaded chitosan nanoparticles (50 mg/kg), according to group allocation.

At the end of the experimental period (after completion of the hypoxia protocol), a single blood sample was collected from the tail vein. When an adequate volume could not be obtained, blood was collected by terminal cardiac puncture under anesthesia. Samples were centrifuged at 3500–4000 rpm for 10 min at 4 °C, and serum was aliquoted and stored at −80 °C until analysis. All measurements were performed in duplicate and read at 450 nm. Hemolyzed samples or those with insufficient volume were excluded.

Biochemical Analyses

Oxidative Stress and Antioxidant Enzyme Analyses in Brain Tissue

At the end of the experiment, rat brain tissues were excised, homogenized in cold phosphate-buffered saline (PBS, pH 7.4), and centrifuged at 10,000 rpm for 10 min to obtain supernatants. Lipid peroxidation and antioxidant enzyme activities in the supernatants were measured using commercial ELISA kits. Malondialdehyde (MDA) levels (Cat no: E0156Ra, BT-LAB), superoxide dismutase (SOD) activity (Cat no: E0168Ra, BT-LAB), and glutathione (GSH) levels (Cat no: E1101Ra, BT-LAB) were Biochemical parameters were expressed as follows: MDA (nmol/mL tissue), SOD (ng/mL tissue), and GSH (mg/L).

Serum Cytokine Levels

To evaluate the inflammatory response in the serum, interleukin-1β (IL-1β) (Cat no: E0119Ra, BT-LAB) and tumor necrosis factor-α (TNF-α) (Cat no: E0764Ra, BT-LAB) levels were measured using commercial ELISA kits. Serum IL-1β and TNF-α concentrations were calculated from standard curves and expressed as ng/L.

Analyses of BDNF, HIF-1α, and iNOS in Brain Tissue

Brain tissue samples obtained from the experimental animals were analyzed for BDNF, HIF-1α, and iNOS levels using the enzyme-linked immunosorbent assay (ELISA) method. Each tissue sample was weighed, homogenized in phosphate-buffered saline (PBS, pH 7.4), and subsequently centrifuged at 4 °C at 10,000 rpm for 15 min. The supernatants obtained were used for analysis. Measurements were performed using species-specific Rat BDNF, HIF-1α, and Results were expressed as BDNF (ng/mL), HIF-1α (pg/mL), and iNOS (pg/mL).

RT-PCR Analysis

Brain tissue samples were isolated according to the protocol of the total RNA (Ecotech Biotech, Turkey) kit, and the RNA quality was assessed using a NanoDrop spectrophotometer (Epoch). Subsequently, cDNA synthesis from RNA was performed using reverse transcriptase enzyme (Ecotech Biotech, Turkey). Real-time quantitative PCR (Rotor Gene Qiagen) analysis was performed using SYBR Green Master Mix (Ecotech Biotech., Turkey) to determine gene expression levels. The expression levels of pro-apoptotic (Caspase-3), anti-apoptotic (Bcl-2), oxidative stress (HO-1, NRF2), and inflammatory (NF-κB, TNF-α), as well as beta actin (internal control) genes (Table 1) were evaluated in the study. Each reaction was run in three technical replicates, and the results were normalized using the $2^{-\Delta\Delta Ct}$ method. Ct values were compared relative to the β-actin (internal control) gene. Melting curve analysis was performed to confirm specificity, and the presence of a single peak was affirmed (Table 1).

Histopathological Examination

Brain tissues from rats in all experimental groups were harvested during systemic necropsy and immediately fixed in 10% neutral buffered formalin for 72 h; following fixation, specimens were dehydrated through a graded ethanol series (50%, 70%, 80%, 96%, and 100%), cleared in xylene, and processed for paraffin infiltration and embedding, after which paraffin blocks were sectioned at 5 µm using a microtome (RM2125 RTS), mounted on glass slides, and

Table 1 Primer sequences and biological functions of genes used in RT-PCR analysis

Gene name	Forward primer (5′→3′)	Reverse primer (5′→3′)	Function/description
Caspase-3	GGT ATT GAG ACA GAC AGT GG	CAT GGG ATC TGT TTC TTT GC	Pro-apoptotic effector; acts in the final stage of cell apoptosis
Bcl-2	CCTGTGGATGACTGAGTACCTG	AGCCAGGAGAAATCAAACAGAGG	Anti-apoptotic gene; protects the cell from apoptosis
HO-1	CTATCGTGCTCGCATGAAC	CAGCTCCTCAAACAGCTCAA	Important in the oxidative stress response; protective effect on the cell via heme oxygenase-1
NRF2	AGTGGATCTGCCAACTACTC	CGAAGCTCATAGTCCTGCTC	Antioxidant response transcription factor; activates HO-1, etc., genes under stress
NF-κB	CGTGAGGCTGTTTGGTTTGA	TCTGCCCTCCTGACTCTACT	Inflammatory gene regulation plays a critical role in immune and stress response
TNF-α	TGATCGGTCCCAACAAGGA	TGCTTGGTGGTTTGCTACGA	Pro-inflammatory cytokine; may trigger inflammation and cell death
Beta actin	TCCTCCTGAGCGCAAGTACTCT	GCTCAGTAACAGTCCGCCTAGAA	Reference gene used to normalize the amount of intracellular RNA

stained with Crossman's modification of Mallory's triple stain; stained sections were examined and photographed using a modified light microscope (Nikon Eclipse E600) at 200× magnification, and histopathological injury was evaluated in the cerebral cortex and hippocampus using a semi-quantitative scoring approach based on the presence and extent of eosinophilic (degenerating) neurons, perineuronal vacuolization, and perivascular space enlargement/edema (0 = none, 1 = mild, 2 = moderate, 3 = severe) by a histopathologist blinded to group allocation [20–22].

Toluidine Blue (Nissl) Staining of the Hippocampal CA Regions

To further evaluate hypoxia-induced neuronal degeneration in the hippocampus, additional sections were stained with Toluidine Blue. After deparaffinization in xylene (2×5 min) and rehydration through a graded ethanol series (100%, 96%, 80%, and 70%), the sections were rinsed in distilled water and stained with 0.1% Toluidine Blue solution for 2–3 min at room temperature. Excess dye was removed by a brief distilled-water wash, and the sections were dehydrated in 95% and absolute ethanol, cleared in xylene, and mounted with Entellan. The slides were examined under a light microscope (Nikon Eclipse 50i with NIS-Elements software), and neuronal morphology, Nissl body integrity, neuronal degeneration, and pyknotic nucleus formation were assessed in the CA1, CA2, and CA3 regions of the hippocampus [23]. Dark (degenerating) neuron density was evaluated by two independent researchers blinded to group allocation.

Immunohistochemical Analysis and Evaluation

Before starting immunohistochemical staining, sections taken on positively charged slides were incubated overnight at 37 °C. Then, the sections were deparaffinized by incubation in two separate xylene solutions for 15 min each. The deparaffinized sections were dehydrated by incubation in 100%, 96%, 80%, and 70% ethyl alcohol series for 5 min each, and then rinsed in distilled water before proceeding to the immunohistochemical staining steps. The prepared slides were boiled in a microwave oven at 600 watts for 4×5 min with citrate solution (pH: 6.0) to reveal the antigen in the tissues. After cooling to room temperature, the slides were washed with PBS, then placed in 3% H_2O_2 for 10 min in a dark environment at room temperature for endogenous peroxidase inactivation. They were then washed with PBS and treated with a protein-blocking solution for 5 min. Following this, they were incubated overnight at +4 °C with primary antibodies anti-NF-κB p65 (Santa Cruz, sc-8008, 1/75 dilution). The slides, washed with PBS, were then treated with secondary antibody and then HRP for 30 min each (washing with PBS between the two solutions). The secondary antibody (Large Volume Detection System: anti-Polyvalent) and HRP (Thermo Fisher Scientific, TP-125-HL) were used as recommended by the manufacturer. DAB (Thermo Fisher, 3,3′-Diaminobenzidine) was used as a chromogen on the slides, washed with PBS. After counterstaining with Mayer's Hematoxylin, the specimens were covered with Entellan and examined under a light microscope. After completing the immunohistochemical procedures, they were evaluated and photographed under a light microscope (Nikon Eclipse E600) at appropriate magnifications. Staining intensity analysis was performed by selecting five different microscopic fields in the sections. The preparations were evaluated by a histopathology specialist and numerically scored according to the staining intensity (0, 1, 2, 3) and the percentage of positively stained cells (0 = 0%, 1 = 1–33%, 2 = 34–66%, 3 ≥ 66%) [24, 25].

Statistical Analyses

All statistical analyses were performed using SPSS 20.0 (IBM Corp., Armonk, NY, USA). Normality and homogeneity of variance were assessed before group comparisons. Continuous variables were compared using one-way ANOVA followed by Tukey's post-hoc test. Histopathological injury scores (0–3) were analyzed using the Kruskal–Wallis test followed by Dunn's post-hoc test for multiple comparisons. Continuous data are presented as mean ± SD, whereas histopathological and immunohistochemical scores are presented as median (IQR). A total of $n = 6$ rats were analyzed per group, and $p < 0.05$ was considered statistically significant.

Results

Characterization of CNPs and CNPs/Orientin

The FT-IR spectra of Orientin, CNPs and CNPs/Orientin are shown in Fig. 1A. In the CNPs and CNPs/Orientin spectra,

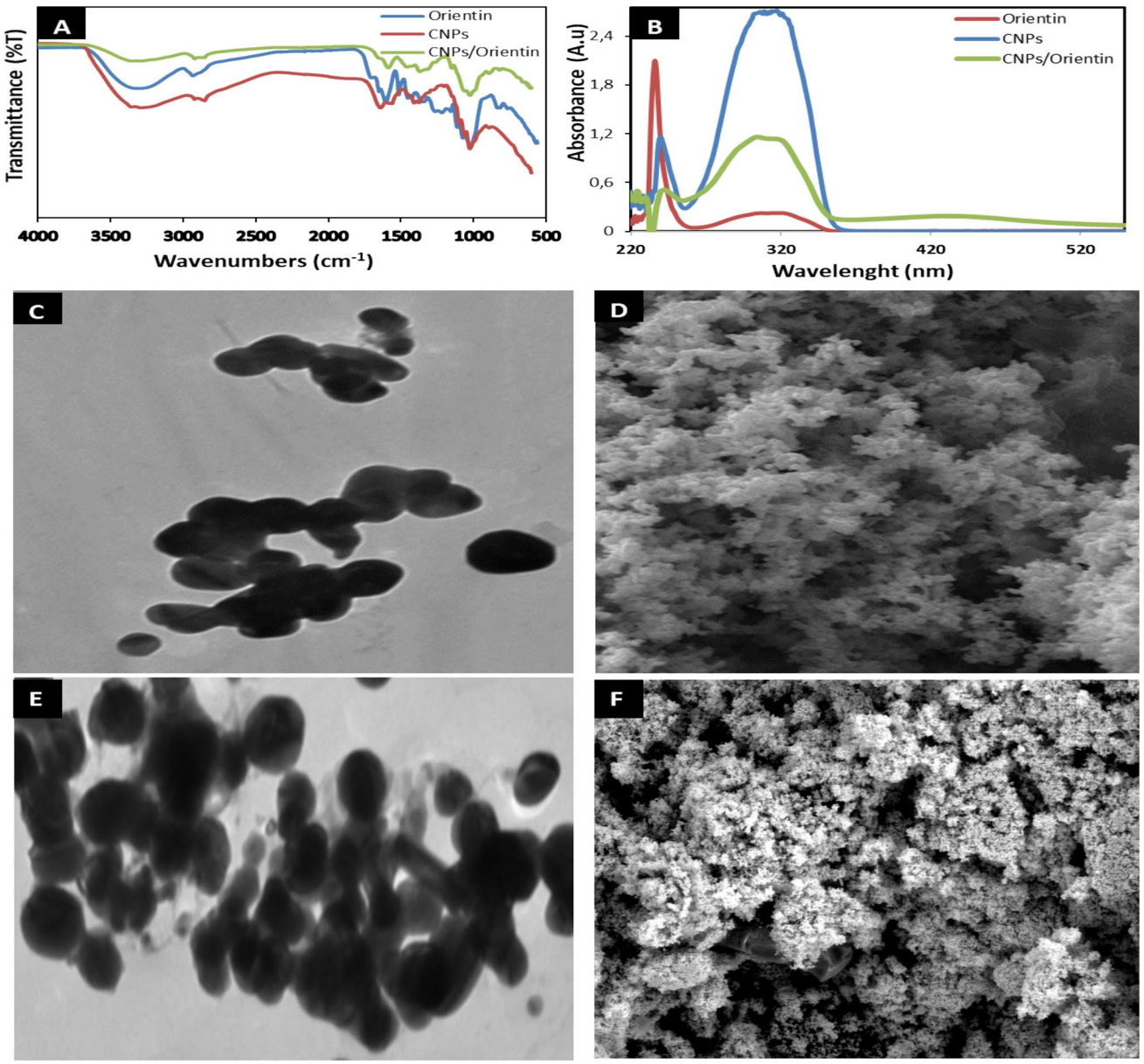

Fig. 1 FT-IR, UV–Vis, TEM, and SEM analyses of the characterization of CNPs and Orientin-loaded CNPs. **A** FT-IR spectra of Orientin, CNPs and CNPs/Orientin. **B** UV–Vis absorption graphs of CNPs and CNPs/Orientin structures. **C** TEM image of CNPs. **D** SEM image of CNPs. **E** TEM image of CNPs/Orientin. **F** SEM image of CNPs/Orientin

approximately combined stretching vibrations belonging to amine (NH_2) and hydroxyl (OH) groups, 3400 cm^{-1}, C–H stretching at 2900 cm^{-1}, carbonyl (C = O) vibration at 1630 cm^{-1}, and N–H deformation vibration at 1370 cm^{-1} were recorded. Additionally, C = O and C = C bands were observed at 275, 1266, 764, 750, and 579 cm^{-1}.

In the UV–Vis analysis, a characteristic absorption peak for CNPs was observed at approximately 270 nm (Fig. 1B). TEM images revealed that CNPs and CNPs/Orientin had a spherical morphology and that particle sizes ranged from 20 to 250 nm (Fig. 1C, E). SEM analysis of CNPs and CNPs/Orientin (Fig. 1D, F) confirmed the formation of well-dispersed nanoparticles with a relatively uniform size distribution.

The results of particle size, PDI, and zeta potential analyses of chitosan nanoparticles are presented in Fig. 2. Dynamic light scattering (DLS) analysis demonstrated that the prepared CNPs and CNPs/Orientin possessed mean hydrodynamic diameters (Z-average) of 235.1 ± 4.9 nm and 245.0 ± 0.7 nm, respectively (Fig. 2A, C). The corresponding polydispersity index (PDI) values were 0.120 ± 0.002 and 0.156 ± 0.009, respectively (Fig. 2A, C), indicating a relatively narrow particle size distribution and successful orientin incorporation without substantial particle aggregation. The low PDI value (<0.2) indicates a narrow particle size distribution and confirms the formation of a highly homogeneous nanoparticle population with minimal aggregation. Furthermore, the small standard deviations obtained among replicate measurements highlight the reproducibility and reliability of the preparation method [26, 27].

Zeta potential measurements revealed that CNPs and CNPs/Orientin exhibited positive surface charges of +30.2 ± 1.8 mV and +29.0 ± 1.3 mV, respectively (Fig. 2B, D). The positive zeta potential values are attributed to the protonation of amino groups on the chitosan backbone and indicate good colloidal stability of the nanoparticle formulations. A zeta potential value approaching +30 mV is generally considered indicative of sufficient electrostatic stabilization, suggesting that the nanoparticles possess good colloidal stability in aqueous media. Consistent with the particle size distribution results, the zeta potential data indicate that the nanoparticles remained well dispersed with a low tendency toward aggregation [15, 26]. Collectively, these findings demonstrate the successful fabrication of chitosan nanoparticles with favorable physicochemical characteristics, including nanoscale size, narrow size distribution, and high colloidal stability. Such properties are particularly advantageous for drug delivery and other biomedical

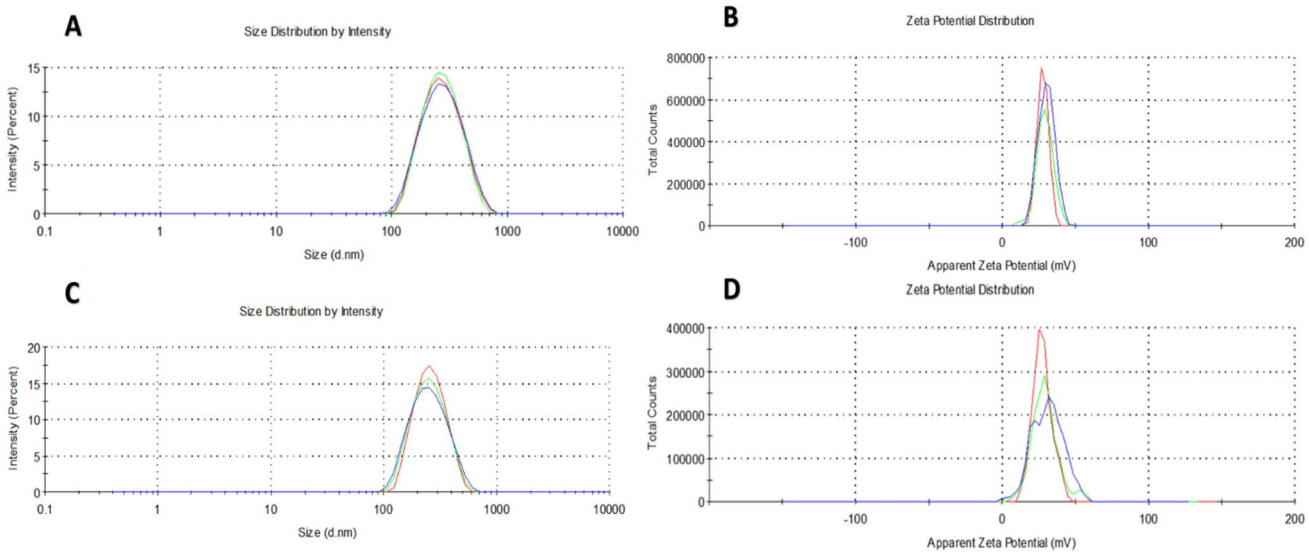

Fig. 2 Dynamic light scattering (DLS) and zeta potential analysis of CNPs (**A**, **B**). DLS and zeta potential analysis of CNPs/Orientin (**C**, **D**)

Table 2 Size and zeta potential values of CNPs and CNPs/Orientin

Nanoparticle	Particle size (nm) (Mean ± SD)	Zeta potential (mV) (Mean ± SD)	Polydispersity index(PDI) (Mean ± SD)	Encapsulation efficiency(%) (Mean ± SD)	Drug loading (%) (Mean ± SD)
CNPs	235.1 ± 4.9	+30.2 ± 1.8	0.120 ± 0.002	_	_
CNPs/Orientin	245.0 ± 0.7	+29.0 ± 1.3	0.156 ± 0.009	81.27 ± 2.4	12.4 ± 0.8

applications, where particle uniformity and stability play critical roles in determining biological performance and therapeutic efficacy (Table 2).

In Vitro Release Study

The in vitro release profile of orientin from chitosan nanoparticles was evaluated under physiological conditions for 72 h (Fig. 3). An initial release of approximately 8.5 ± 1.2% was observed within the first 30 min, followed by a gradual increase to 12.8 ± 1.4% at 1 h, 21.6 ± 1.8% at 3 h, and 31.4 ± 2.1% at 6 h. Thereafter, orientin was released in a sustained manner, reaching 43.2 ± 2.3% at 12 h, 57.8 ± 2.6% at 24 h, 71.5 ± 2.4% at 48 h, and 79.6 ± 3.0% after 72 h. The delayed release observed after 72 h can be attributed not only to the strong interactions between orientin and the chitosan matrix but also to the gradual diffusion of the drug through the polymeric network. Consequently, these findings demonstrate that the prepared chitosan nanoparticles provide an effective sustained-release platform for orientin delivery [28].

Results of Biochemical Analyses

Oxidative Stress Findings

In the hypoxia group, superoxide dismutase (SOD) and glutathione (GSH) levels were significantly reduced (SOD: $p < 0.001$; GSH: $p < 0.001$), while malondialdehyde (MDA) levels were prominently increased ($p < 0.001$). Single applications of CNPs and Orientin provided a partial improvement in SOD and GSH levels ($p < 0.05$ for both), while the CNPs + Orientin combination significantly suppressed the adverse effects associated with hypoxia. Specifically, in the Hypoxia + CNPs/Orientin group, SOD and GSH levels rose to levels similar to the control group ($p < 0.001$), while MDA levels were found to be significantly reduced ($p < 0.001$) (Fig. 4).

Serum Cytokine Levels

When IL-1β levels were evaluated, a significant increase was observed in the hypoxia group ($p < 0.001$, letter: b), indicating a marked increase in the inflammatory response. All other groups (Control, Orientin, CNPs, CNPs+Orientin, Hypoxia+Orientin, Hypoxia+CNPs, Hypoxia+CNPs/Orientin) were classified within the "a" letter group, showing no statistically significant differences among them ($p > 0.05$). When TNF-α levels were similarly analyzed in Graph B, only the hypoxia group was found to produce significantly higher levels of TNF-α than the other groups ($p < 0.001$, letter: b). All other groups remained at statistically similar levels in terms of TNF-α levels ($p > 0.05$, letter: a) (Fig. 5).

BDNF, HIF-1α, and iNOS Levels in Brain Tissue

BDNF levels were significantly reduced in brain tissue samples from rats exposed to hypoxia compared to the control group ($p < 0.01$). In contrast, significant increases were observed in HIF-1α ($p < 0.01$) and iNOS ($p < 0.001$) levels. BDNF levels in the groups that only received Orientin or CNPs appeared similar to the control group ($p > 0.05$), and no significant difference was observed in HIF-1α and iNOS levels compared to the control group ($p > 0.05$). A

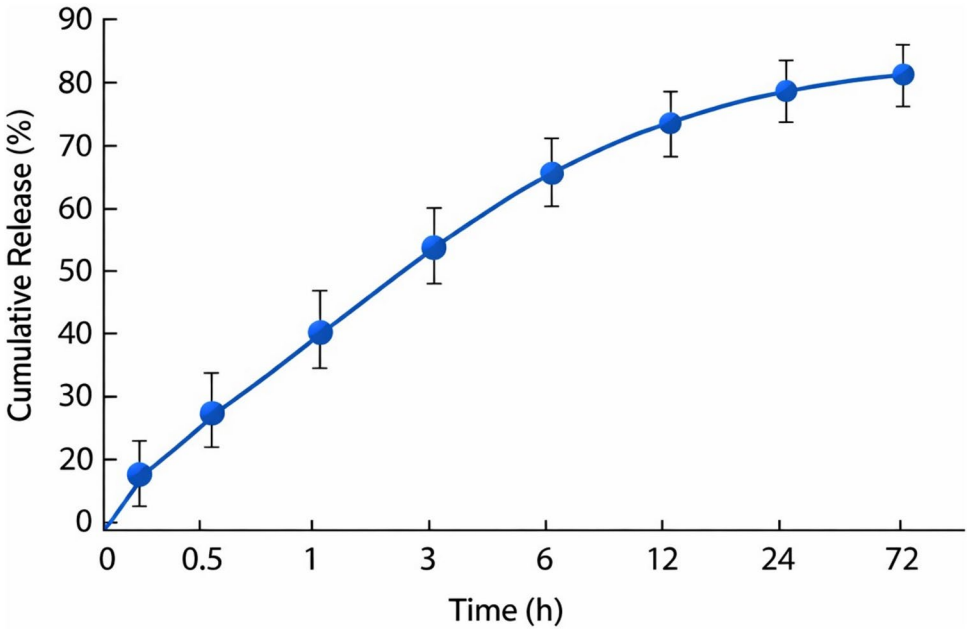

Fig. 3 In vitro cumulative release profile of orientin from chitosan nanoparticles over 72 h

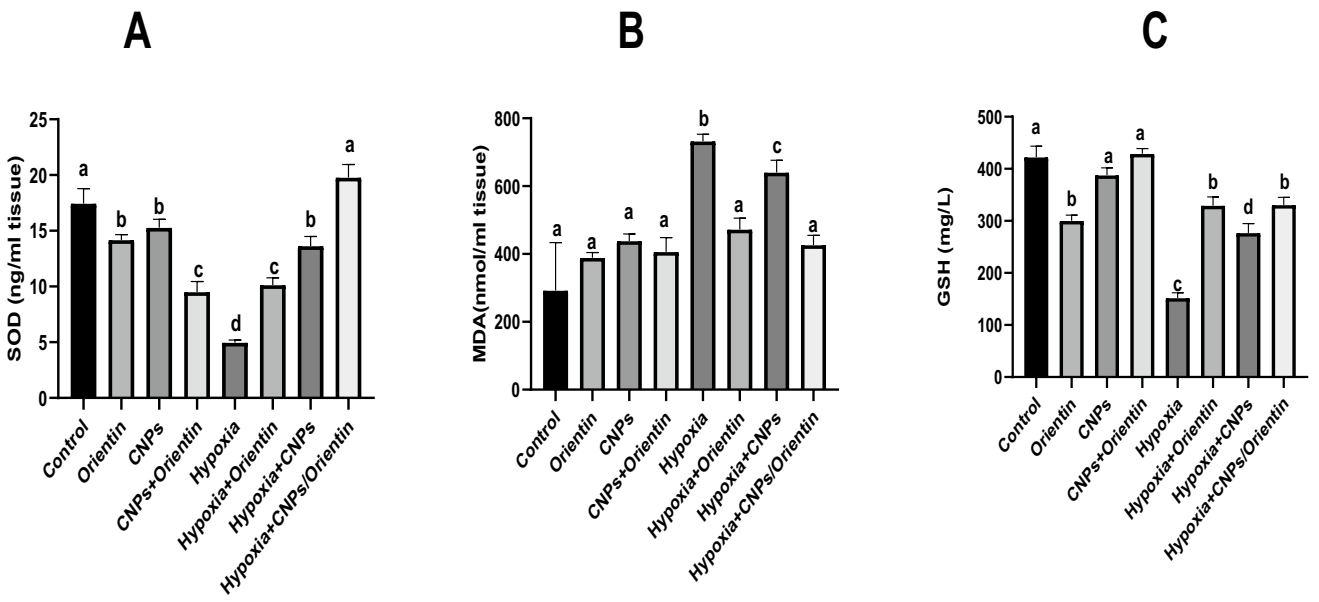

Fig. 4 Distribution of MDA, SOD, and GSH levels in brain tissues according to experimental groups. Treatments containing orientin and CNPs reduced these effects, thereby alleviating oxidative damage. Data are presented as mean ± SD ($n = 6$, $p < 0.05$)

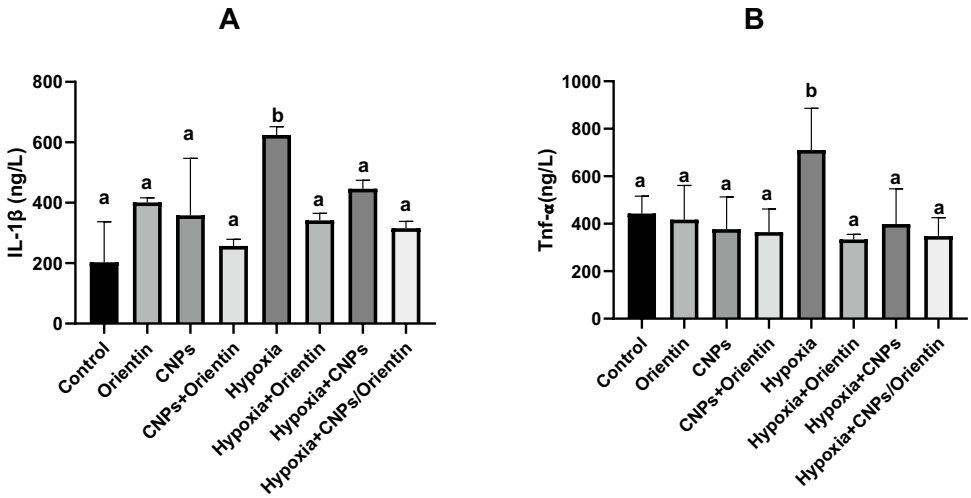

Fig. 5 Evaluation of inflammatory cytokine levels in serum **A** IL-1β and **B** TNF-α levels

significant increase in BDNF levels ($p < 0.05$) was observed in the Hypoxia+Orientin, Hypoxia+CNPs, and especially Hypoxia+CNPs/Orientin groups, whereas a significant decrease in HIF-1α ($p < 0.05$) and iNOS ($p < 0.01$) levels was observed. The most significant change was observed in the Hypoxia+CNPs/Orientin group; in this group, BDNF levels approached control values, while HIF-1α and iNOS levels were significantly lower compared to other treatment groups ($p < 0.05$) (Fig. 6).

Rt-PCR Results

In the evaluation of RT-PCR data, hypoxia treatment resulted in significant changes in the expression of caspase-3, Bcl-2, HO-1, NRF2, NF-κB, and TNF-α genes ($p < 0.05$). Caspase-3 and TNF-α expression increased significantly in the hypoxia group (***$p < 0.001$, ****$p < 0.0001$). Anti-apoptotic Bcl-2 was significantly increased in the hypoxia group (**$p < 0.01$, ****$p < 0.0001$), and HO-1 and NRF2 expression were also significantly enhanced under hypoxia (****$p < 0.0001$). NF-κB levels were significantly increased in the hypoxia group (*$p < 0.05$, ***$p < 0.001$, ****$p < 0.0001$), whereas orientin and CNPs alone did not show a significant effect. However, the combinations of hypoxia+CNPs, hypoxia+Orientin, and hypoxia+CNPs/Orientin reduced the expression levels of TNF-α, NF-κB, and caspase-3 compared to hypoxia. RT-PCR expression profiles and comparisons for all groups are presented in Fig. 7.

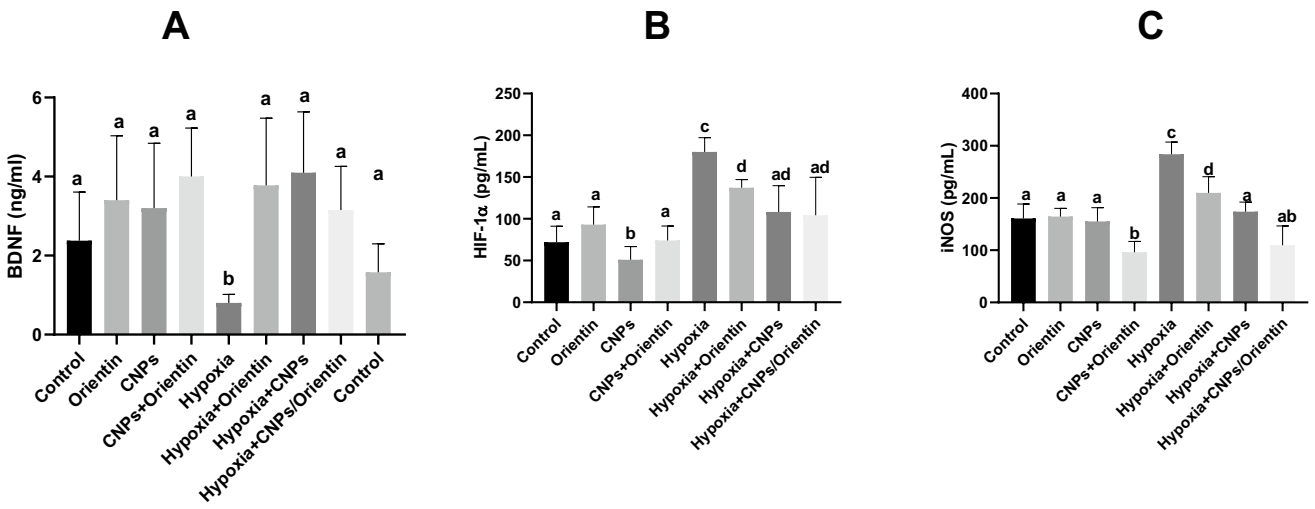

Fig. 6 Levels of BDNF (**A**), HIF-1α (**B**), and iNOS (**C**) in hypoxic rat brain tissue. Hypoxia decreased BDNF while increasing HIF-1α and iNOS ($p < 0.01$). Orientin, CNPs, and their combinations reversed these changes ($p < 0.05$). Different letters indicate statistical significance ($p < 0.05$)

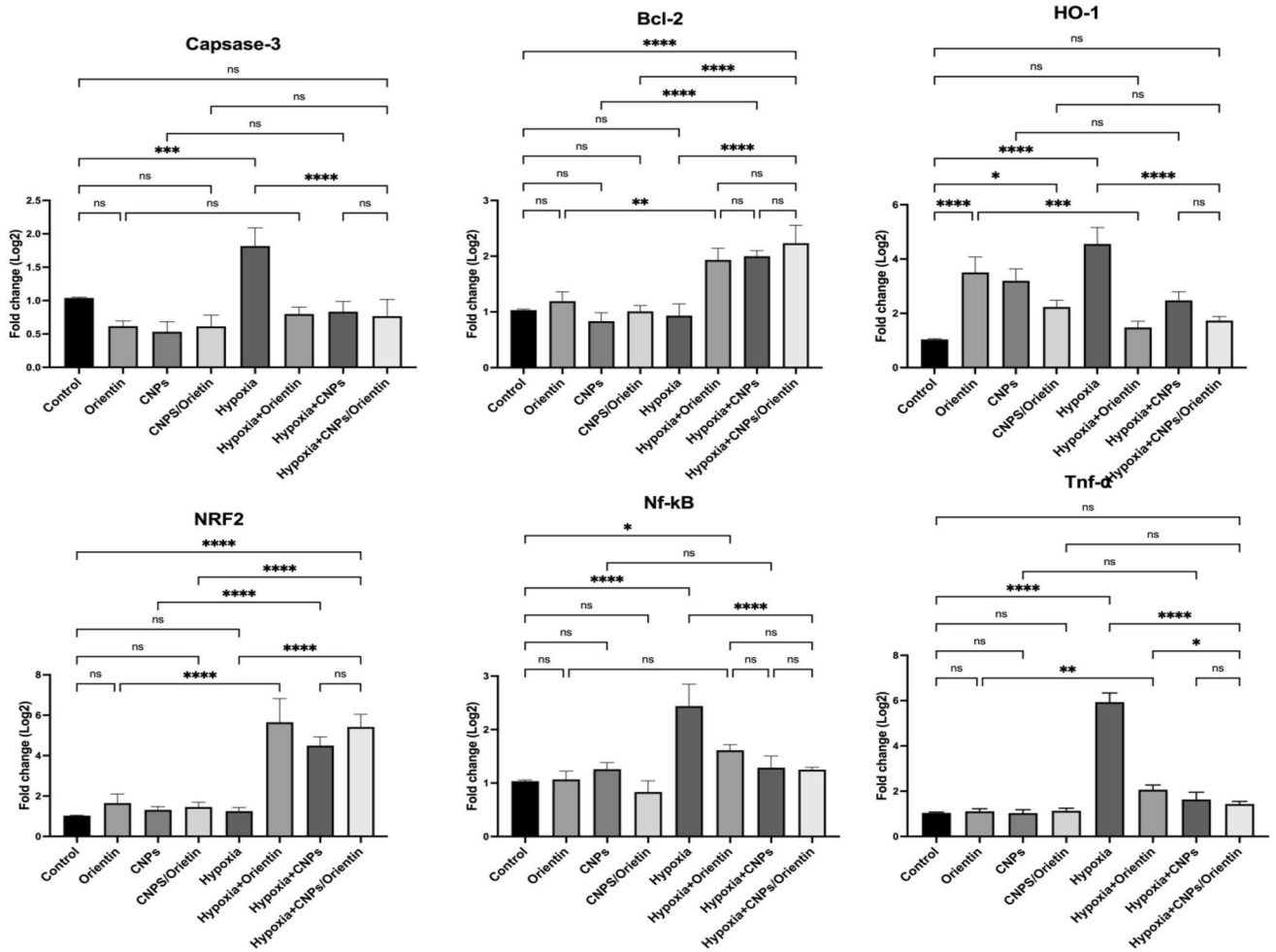

Fig. 7 Caspase-3, Bcl-2, HO-1, NRF2, NF-κB, and TNF-α gene expression data for rat brain tissue application groups. Data are presented as mean ± SD. Statistical analysis was performed using one-way ANOVA and Tukey multiple comparison test. *$p < 0.05$, **$p < 0.01$, ***$p < 0.001$, ****$p < 0.0001$, ns: insignificant

Scoring of Brain Injury

When brain tissue was examined, no histopathological alterations were detected in the Control, CNPs, Orientin, and CNPs-Orientin groups, and all samples exhibited a normal histological appearance. In the Hypoxia group, most neurons in the cerebral cortex showed acidophilic staining, accompanied by pronounced perineuronal vacuolization and expansion in the perivascular areas. Acidophilic degenerative neurons were also observed in the hippocampal region. In the Hypoxia+CNPs, Hypoxia+Orientin, and Hypoxia+CNPs/Orientin groups, histopathological lesions were markedly reduced in both the cerebral cortex and hippocampus compared with the Hypoxia group. Notably, the lesions remained most limited in the Hypoxia+CNPs/Orientin group. All findings are presented in Figs. 8, 9, and 10.

Toluidine Blue Staining of the Hippocampal CA Regions

Histopathological examination of the hippocampus by Toluidine Blue staining revealed that, compared with the control group, dark neuron density was markedly increased in the CA1 and CA3 regions of the hypoxia group ($p < 0.0001$).

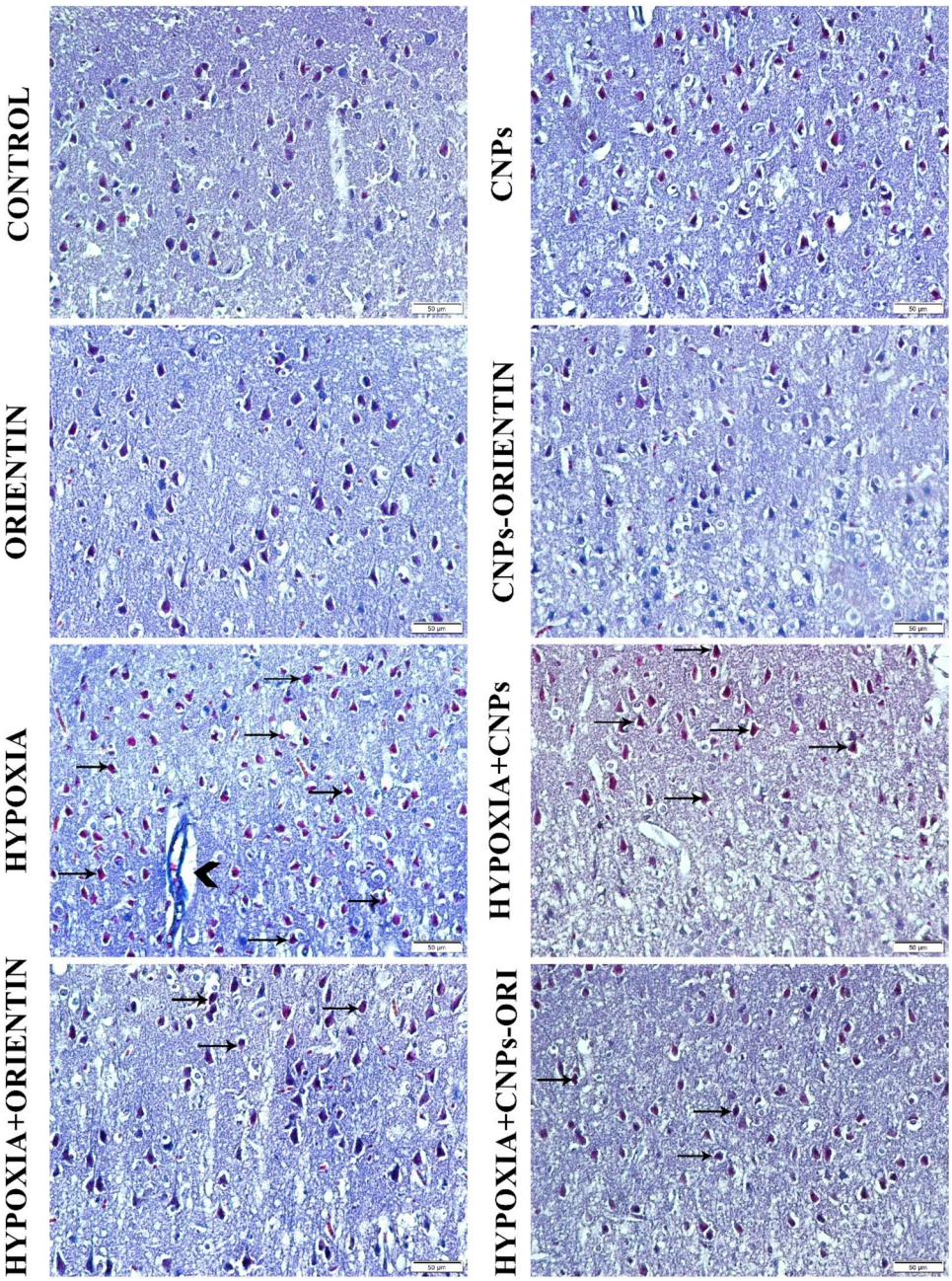

Fig. 8 Cerebral cortex micrographs from all groups (Crossman's modification of Mallory's triple stain, ×200 magnification). Arrowhead: Perivascular expansion, arrow: Acidophilic degenerative neurons and perineuronal vacuolization

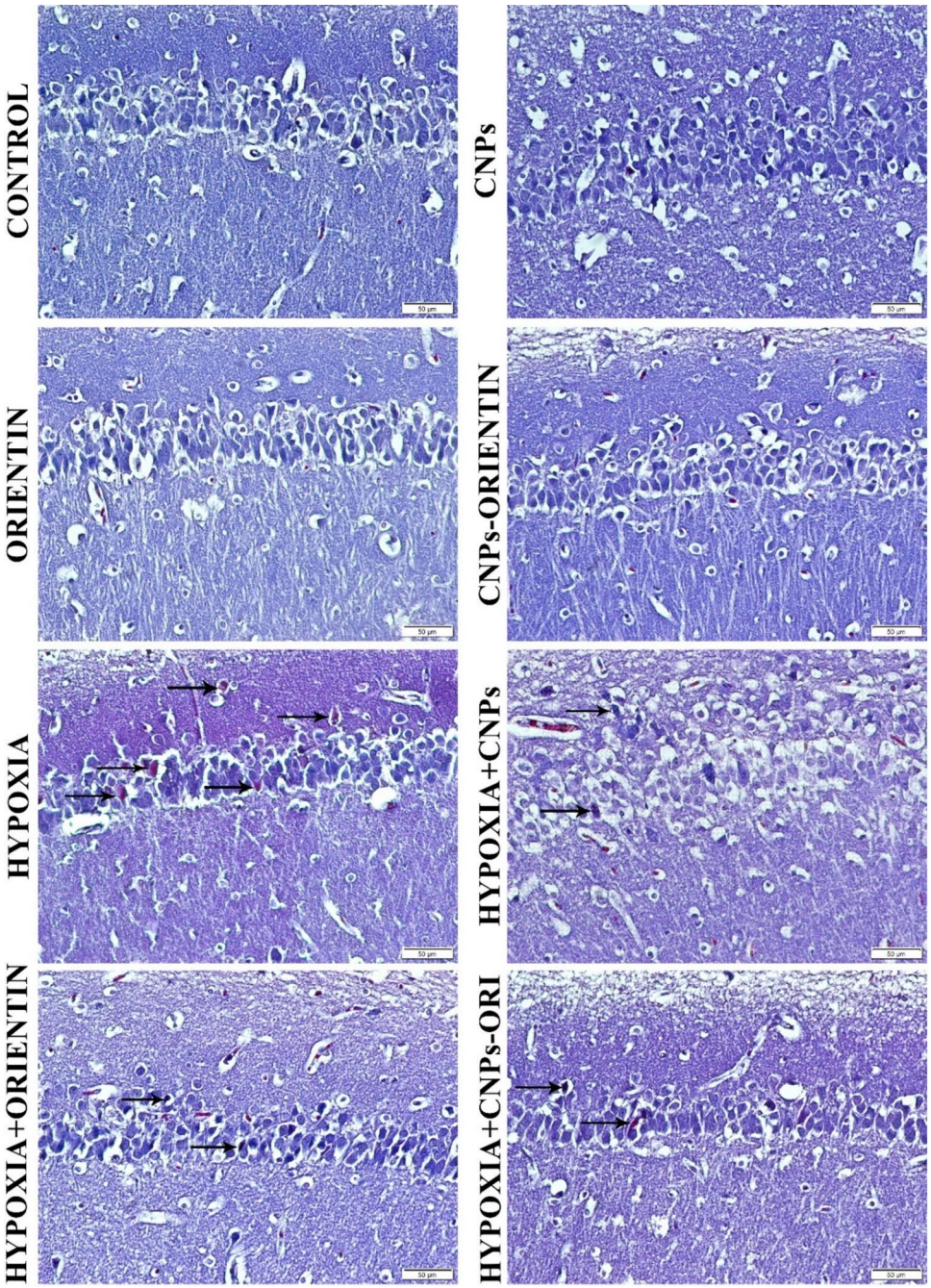

Fig. 9 Hippocampal micrographs of all groups (Crossman's modification of Mallory's triple stain, ×200 magnification). Arrow: Acidophilic degenerative neurons

Orientin and, most notably, CNPs/Orientin treatment significantly reduced the hypoxia-induced increase in dark neuron density, with the most pronounced improvement observed in the CNPs/Orientin group. In the CA2 region, although dark neuron density increased with hypoxia, no significant difference was detected among the post-hypoxia treatment groups ($p > 0.05$). These findings indicate that hypoxia-induced neuronal degeneration is more prominent in the CA1 and CA3 regions and that CNPs-delivered Orientin exerts a neuroprotective effect against this degeneration. A representative hippocampal image with the CA1, CA2, and CA3 regions annotated is presented in Fig. 11, and the corresponding micrographs and statistical evaluation are presented in Figs. 12 and 13.

Immunohistochemical Findings

Immunohistochemical stainings of the hippocampus and cortex regions in brain tissues from all groups were visualized under a light microscope at 200× magnification and evaluated and presented. Immunoreactivity to the NF-kB-p65 antibody increased in both regions in the Hypoxia group

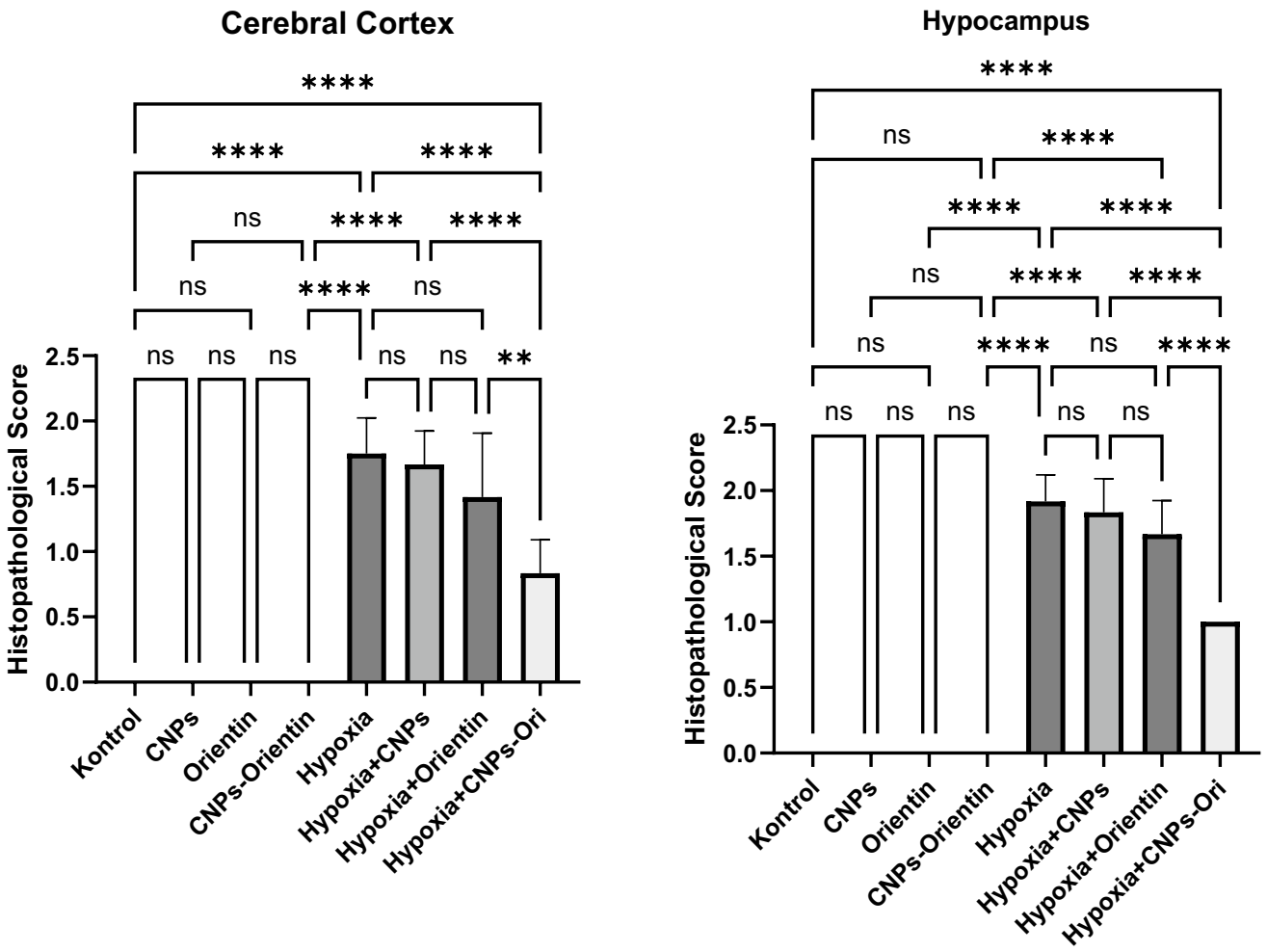

Fig. 10 Evaluation of brain cerebral cortex and hippocampus histology. Values are presented as median (IQR) ($n=6$). Groups were compared using the Kruskal–Wallis test followed by Dunn's post-hoc test for multiple comparisons. *$p<0.05$; **$p<0.01$; ***$p<0.001$; ****$p<0.0001$. The reduction in histopathological injury scores in the Hypoxia+CNPs/Orientin group was consistent with the observed normalization of oxidative stress markers and apoptotic gene expression

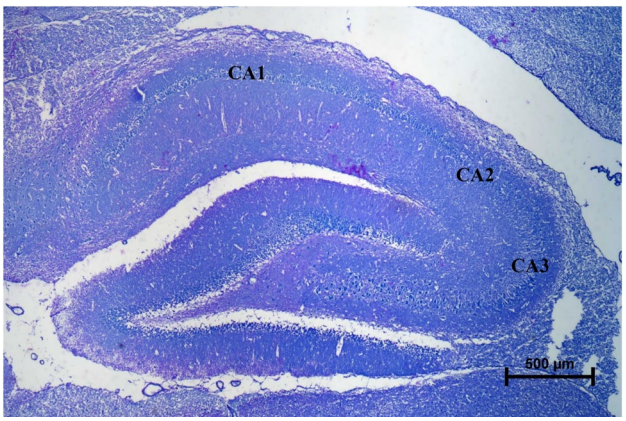

Fig. 11 Rat brain hippocampal region (Toluidine Blue staining, magnification×40). CA, Cornu Ammonis

compared to the control groups, while it decreased in the treatment groups, especially in the Hypoxia+CNPs+ORI group. Immunohistochemical stainings for all groups are presented in Figs. 14 and 15, and the statistical evaluation is presented in Fig. 16.

Discussion

Hypoxic brain injury is a complex process driven by intertwined oxidative stress and inflammatory activation, leading to disrupted redox homeostasis, lipid peroxidation, and progressive neuronal damage [29, 30].

In this study, a significant decrease in SOD and GSH levels and a marked increase in MDA levels ($p<0.001$) were observed in the hypoxia group (Fig. 4), confirming that oxidative stress plays a central role in hypoxic brain injury.

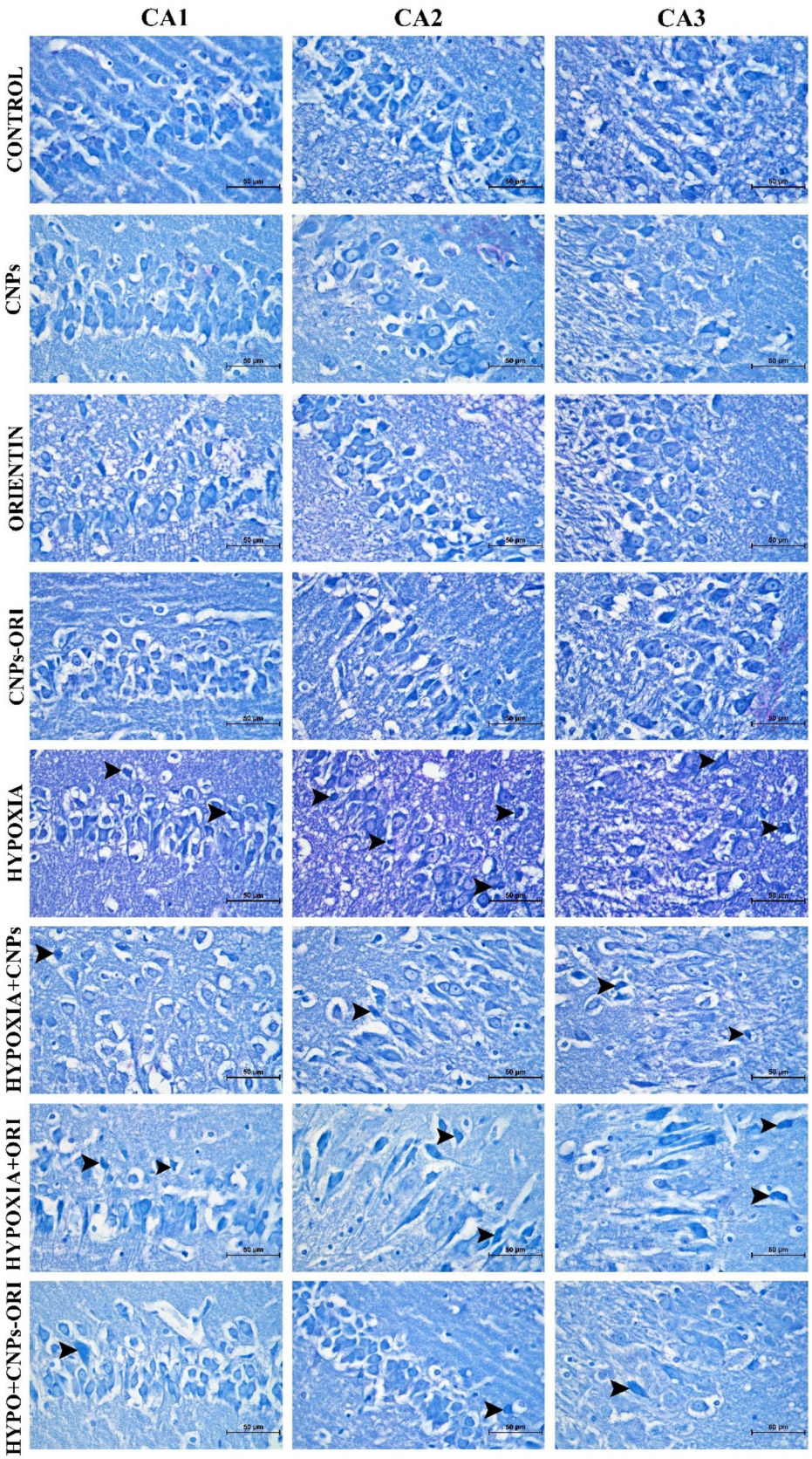

Fig. 12 Micrographs of the hippocampal regions of all groups (Toluidine Blue, magnification × 600). Arrowhead: degenerative neurons

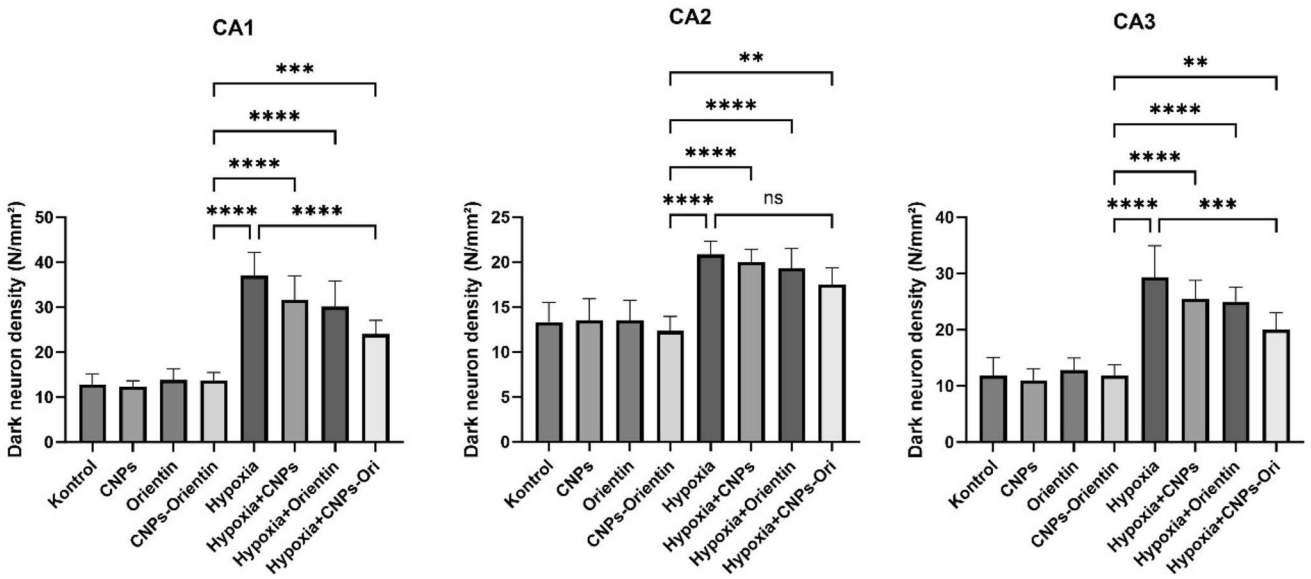

Fig. 13 Evaluation of Cornu Ammonis histology. Values are presented as mean ± SD ($n = 6$) and were analyzed by one-way ANOVA followed by Tukey's test. Asterisks (*$p < 0.05$; **$p < 0.01$; ***$p < 0.001$; ****$p < 0.0001$) indicate statistically significant differences between groups ($p < 0.05$)

Single administration of orientin or CNPs was associated with partial improvement in oxidative stress markers, including increases in SOD and GSH ($p < 0.05$) and a reduction in MDA. However, these parameters did not reach the levels of the control group.

The literature reports that Orientin increases antioxidant capacity, reduces ROS production, and increases SOD activity in different experimental models [9, 10]. Chitosan nanoparticles, while primarily defined as a drug delivery system, have been reported to possess limited radical scavenging effects through functional groups in their structure and to modulate antioxidant enzyme activities [31, 32]. The strongest antioxidant effect was obtained with the combination of CNPs/Orientin. In this group, SOD and GSH levels increased to levels similar to the control group ($p < 0.001$), while MDA levels decreased significantly ($p < 0.001$). The superior efficacy of the combined treatment compared to single administrations is consistent with improved delivery and stabilization of orientin by CNPs; however, direct measurement of orientin concentration in brain tissue was not performed, and increased bioavailability cannot be conclusively demonstrated. Similarly, studies have reported increased bioavailability and antioxidant activity following the formulation of different flavonoids (e.g., quercetin, rutin, resveratrol) with chitosan nanoparticles [33–36]. These results are contextually consistent with the effect observed for Orientin; it has been suggested that this enhanced effect may be related to the activation of the Nrf2/ARE pathway and the facilitating properties of CNPs in crossing the blood–brain barrier [11, 37].

Inflammation was also strongly activated during the hypoxic process, concurrently with oxidative stress. A significant increase in IL-1β and TNF-α levels in the hypoxia group ($p < 0.001$) (Fig. 5) confirms a pronounced pro-inflammatory response, which is consistent with hypoxia-driven cytokine induction mediated, at least in part, through NF-κB signaling [38]. Importantly, all treatment regimens—Orientin, CNPs, and CNPs/Orientin—attenuated these hypoxia-induced cytokine elevations. Cytokine levels in the treated groups were not significantly different from those in controls, and no significant differences were observed among the treatment groups, indicating comparable anti-inflammatory effects.

Although CNPs/Orientin produced greater improvements in oxidative stress, HIF-1α, iNOS, BDNF, and histopathological findings than Orientin alone, no statistically significant superiority was observed for serum IL-1β and TNF-α levels. This finding suggests that, under the present experimental conditions, the anti-inflammatory effect of Orientin may have approached a maximal response, thereby limiting the detection of additional reductions in circulating cytokine levels following nanoparticle delivery. Accordingly, the principal advantage of chitosan nanoparticle-mediated Orientin delivery appears to be reflected predominantly in enhanced antioxidant protection, improved regulation of hypoxia-related molecular pathways, and preservation of neuronal architecture rather than in further suppression of systemic inflammatory cytokines.

Accordingly, while the anti-inflammatory effect at the serum cytokine level was comparable across all treatment

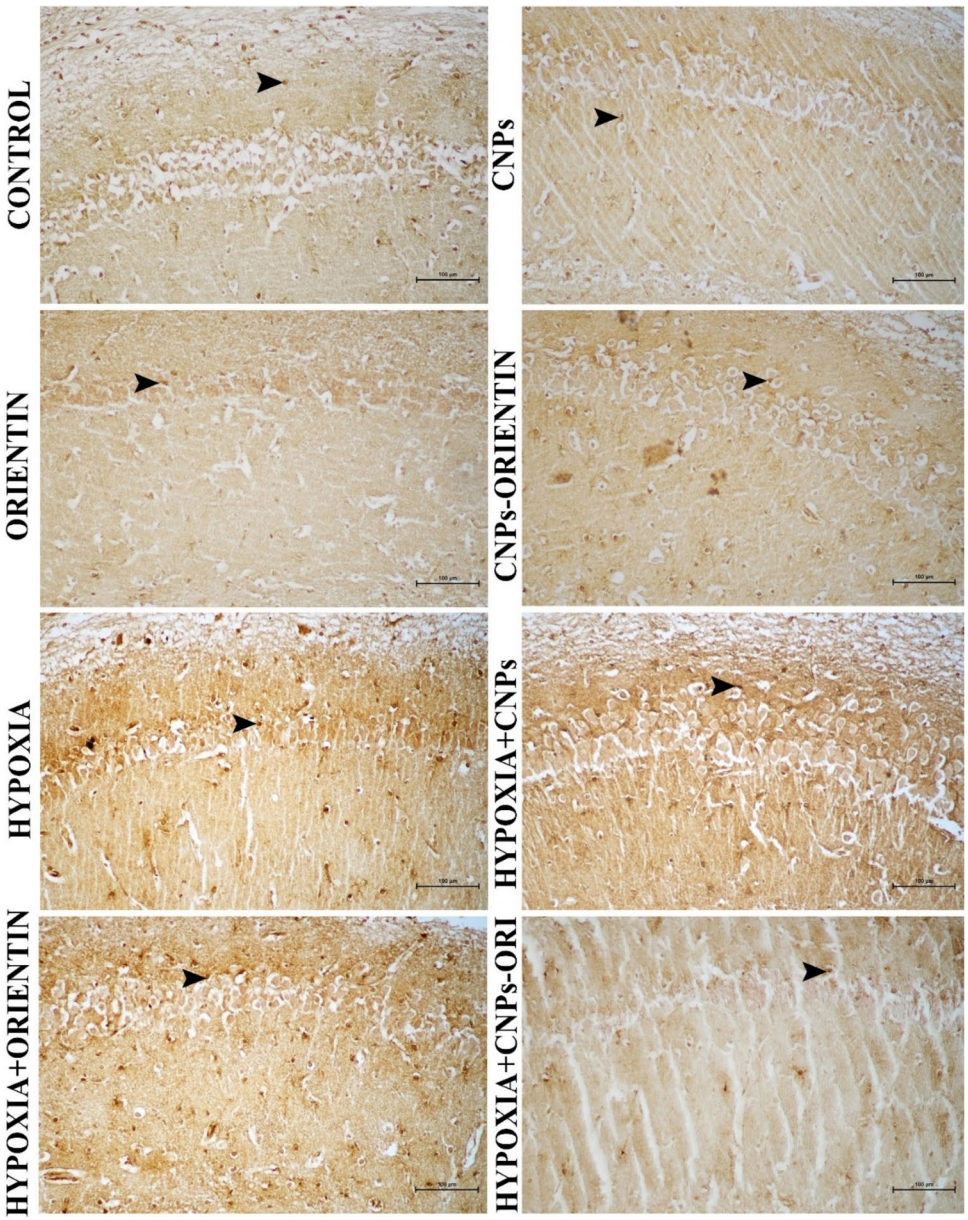

Fig. 14 NF-κB p65 antibody immunoreactivity of hippocampus brain tissue in all groups. Staining; Streptavidin Biotin Peroxidase Method. Magnification; 200×

arms, the superior efficacy of the CNPs/Orientin combination was most evident at the oxidative, structural (histopathological), and NF-κB-related molecular levels. Our study also demonstrated that hypoxia suppresses BDNF-mediated neurotrophic support by inducing the neuronal stress response in brain tissue, while significantly increasing HIF-1α and iNOS expression ($p < 0.01$) (Fig. 6). These changes support activation of HIF-1α-dependent responses under oxygen/energy deprivation, promoting nitrosative stress and neuronal dysfunction [39, 40]. The fact that BDNF levels in brain tissue remained close to the control group in groups treated with Orientin or CNPs alone suggests that these compounds contribute to the preservation of BDNF synthesis by enhancing antioxidant capacity. The free radical scavenging effect of orientin [9] and the bioavailability-enhancing property of chitosan nanoparticles [41] may have facilitated the continuation of neurotrophic support. Notably, the significant increase in BDNF levels ($p < 0.05$) and the marked reductions in HIF-1α ($p < 0.05$) and iNOS ($p < 0.01$) in the Hypoxia+CNPs/Orientin group indicate that this combined treatment most effectively restores BDNF-related neurotrophic support while attenuating HIF-1α/iNOS-associated hypoxic-nitrosative signaling.

RT-PCR analyses demonstrated that oxidative stress–responsive (NRF2/HO-1), inflammation (NF-κB/TNF-α), and apoptosis-related (Caspase-3/Bcl-2) processes are simultaneously altered at the molecular level in hypoxic brain injury (Fig. 7). In the hypoxia group, significant increases in Caspase-3, NF-κB, and TNF-α gene expression were observed ($p < 0.001$–0.0001). These findings indicate

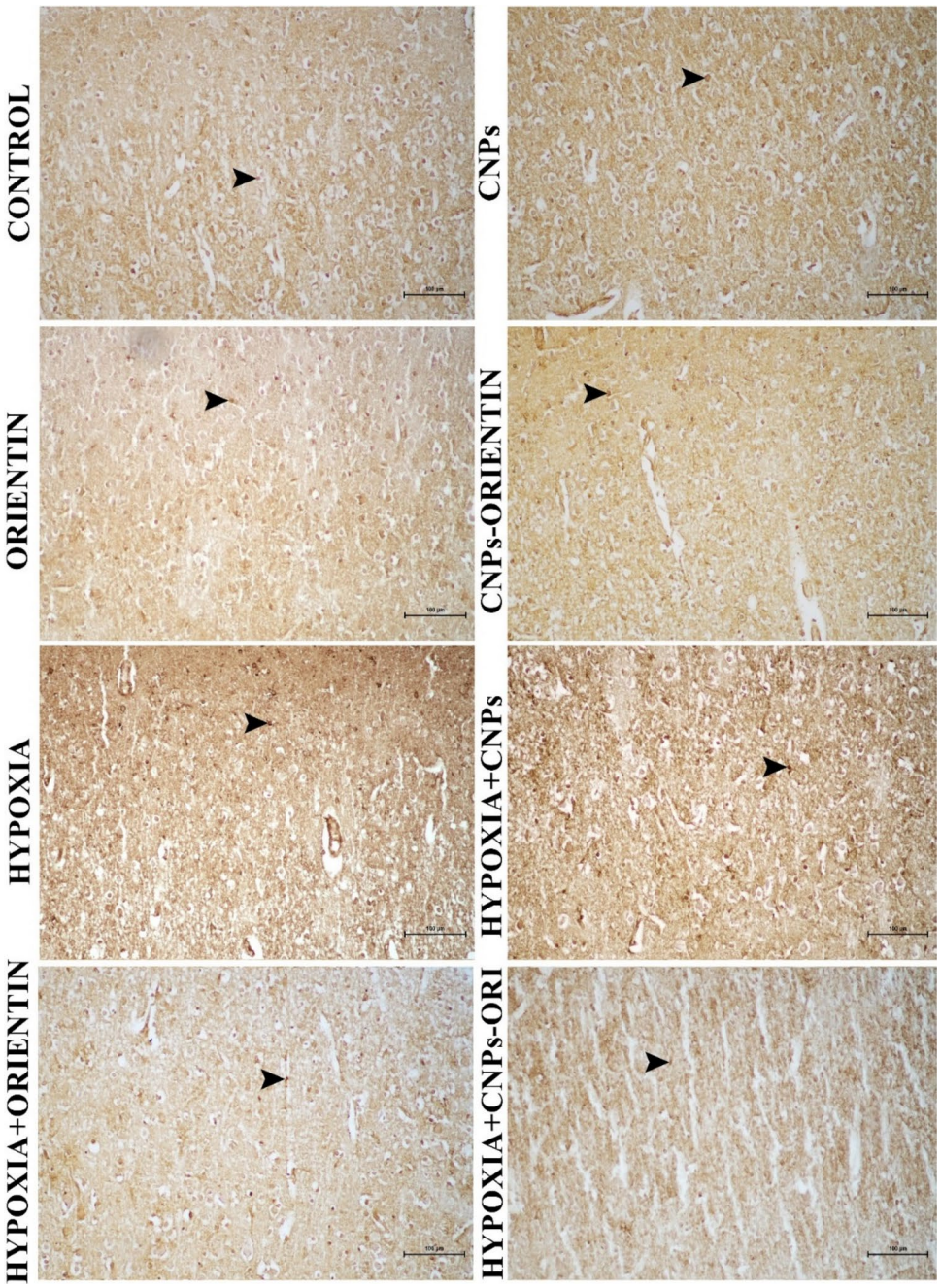

Fig. 15 NF-κB p65 antibody immunoreactivity in the cortical region of brain tissue in all groups. Staining: Streptavidin Biotin Peroxidase Method. Magnification; 200×

that hypoxia concurrently triggers pro-apoptotic and pro-inflammatory responses in brain tissue, suggesting that the cellular death cascade may be amplified by NF-κB–linked cytokine signaling. This pattern is compatible with prior evidence that hypoxia-induced oxidative stress and mitochondrial dysfunction promote Caspase-3 activation [29, 30].

The significant increase in Bcl-2 expression ($p < 0.01$) in the hypoxia group reflects a compensatory anti-apoptotic response; however, the pronounced elevation in Caspase-3 suggests that this defense mechanism is insufficient. Consistent with previous experimental evidence, Caspase-3 activation is closely associated with oxidative stress–driven apoptotic signaling regulated by Nrf2-related pathways, indicating that Caspase-3 acts as a key downstream executor of cellular injury under pathological conditions [42]. Concurrently, the marked increases in HO-1 and NRF2 gene expression (****$p < 0.0001$) indicate activation of the endogenous antioxidant response. Nevertheless, as evidenced by the biochemical findings (SOD ↓, GSH ↓, MDA ↑), the oxidative burden remains dominant.

Single administration of Orientin and CNPs partially restored this balance; while HO-1 and NRF2 activation

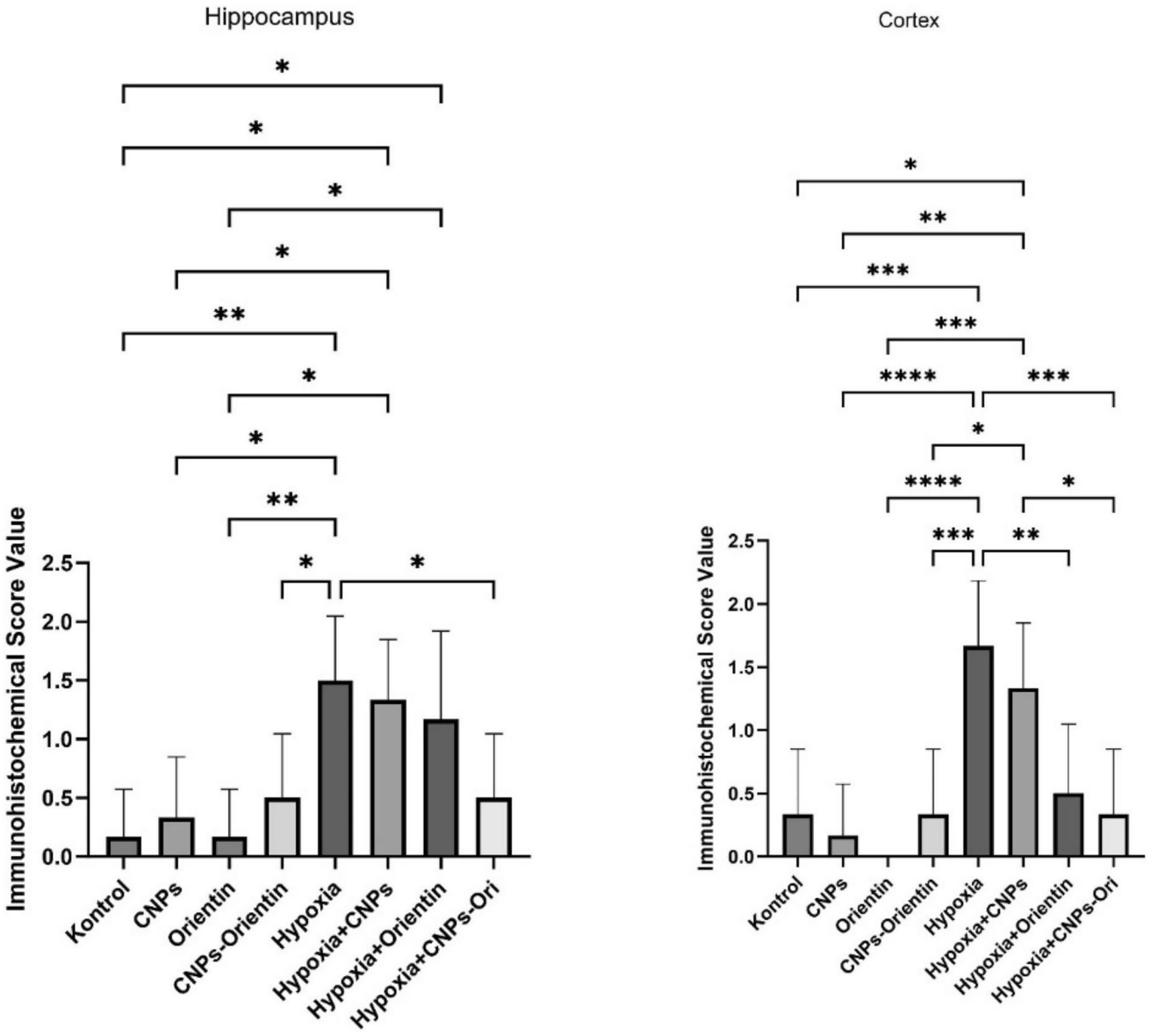

Fig. 16 Immunohistochemical analysis evaluation of NF-κB p65 antibody in hippocampus and cortex regions of brain tissues of all groups. Values are presented as median (IQR) ($n=6$) and were analyzed using the Kruskal–Wallis test followed by Dunn's multiple comparisons test. *$p<0.05$, **$p<0.01$, ***$p<0.001$, ****$p<0.0001$

persisted, a downward trend was observed in the expression of Caspase-3, NF-κB, and TNF-α. However, the most pronounced improvement was seen in the Hypoxia+CNPs/Orientin group. In this group, the increase in pro-apoptotic and pro-inflammatory genes was significantly suppressed ($p<0.05$–0.001), while HO-1 and NRF2 activation persisted and Bcl-2 showed a treatment-associated increase.These findings suggest that the combination treatment produces a more robust antioxidant and anti-inflammatory effect compared with single-agent administration.

It has previously been reported that Orientin increases HO-1 transcription by activating the Nrf2/ARE pathway and suppresses NF-κB activation [9, 10], while CNPs have been reported to enhance the bioavailability and tissue stability of Orientin [31, 32]. The simultaneous activation of HO-1/NRF2 and suppression of NF-κB/TNF-α observed in our study indicates that these two mechanisms act in concert. Thus, the CNPs/Orientin combination provided a dual regulatory effect on the oxidative–inflammatory imbalance induced by hypoxia. Consistent with our findings, recent studies in different experimental models of inflammation have demonstrated that activation of the Nrf2 pathway not only enhances endogenous antioxidant defenses but also suppresses NF-κB-driven inflammatory signaling and

inflammasome-related responses, thereby attenuating tissue injury and apoptosis beyond hypoxic conditions [43, 44].

These coordinated molecular changes are directly parallel with the biochemical improvement observed in the same rats (SOD ↑, GSH ↑, MDA ↓). These regulatory shifts in gene expression are also consistent with the histopathological findings presented in the following section; the preservation of cortical and hippocampal integrity in the combination-therapy group may be related to the attenuation of Caspase-3 and NF-κB signaling. Taken together, the RT-PCR and histopathological data support that the CNPs/Orientin combination limits hypoxia-induced brain injury at both transcriptional and morphological levels.

In accordance with biochemical, immunological, and molecular findings, histopathological examinations revealed that hypoxia causes significant structural damage in brain tissue. In the hypoxia group, perivascular dilation and perineuronal vacuolization in the cerebral cortex were prominent, whereas degenerative neuronal changes were also evident in the hippocampus (Figs. 8, 9, 10). This finding demonstrates that hypoxia creates region-specific vulnerability within the brain; the heightened sensitivity of the hippocampus to oxygen deprivation is consistent with the literature [6, 44]. Consistent with this regional vulnerability, Toluidine Blue staining showed that the hypoxia-induced increase in dark (degenerating) neuron density was significant in the CA1 and CA3 subfields ($p < 0.0001$) and was attenuated by CNPs/Orientin, whereas the CA2 region showed no significant differences among the post-hypoxia treatment groups, indicating a subfield-specific pattern of hypoxic susceptibility and treatment response. While vascular dilation is predominant in cortical lesions, acidophilic degeneration and neuronal loss are predominant in hippocampal regions. When considered together with the simultaneous increases in HIF-1α and iNOS levels, these findings suggest that hypoxia may disrupt endothelial barrier function and induce nitrosative stress–associated neuronal injury [5, 7].

Single administration of Orientin and CNPs partially alleviated this structural damage. The severity of perivascular expansion and vacuolization in the cortex decreased, and the areas of degeneration within the hippocampus were reduced; however, overall structural integrity was not fully preserved. This limited improvement is consistent with the partial decrease in Caspase-3, NF-κB, and TNF-α expression observed at the molecular level. The inability of single treatments to provide complete protection may be attributed to the solubility and bioavailability limitations of Orientin and to the fact that CNPs function primarily as carrier systems and do not possess strong intrinsic antioxidant capacity. These findings parallel studies showing that flavonoids exert neuroprotective, yet not fully restorative, effects when administered alone [8, 45]. Although functional behavioral assessments were not included in this study, the concordant improvement in biochemical, transcriptional, and histopathological parameters strongly supports a biologically meaningful neuroprotective effect. Nevertheless, the use of multiple converging endpoints, including biochemical, molecular, and histopathological analyses, strengthens the internal validity of the findings.

The most pronounced morphological protection was observed in the Hypoxia+CNPs/Orientin combination group. In this group, cortical vascular expansion was markedly reduced, and hippocampal neuronal integrity was better preserved. This histological improvement paralleled the increase in SOD and GSH, decrease in MDA, reductions in HIF-1α and iNOS, and the increase in BDNF levels detected in the same group. Together, these converging findings suggest that combination therapy attenuates vascular and neuronal injury associated with oxidative and nitrosative stress. Furthermore, the HO-1/NRF2 response and the suppression of NF-κB/TNF-α signals observed in RT-PCR analyses are consistent with the molecular context accompanying the preservation of neuronal integrity at the histological level.

In addition, NF-κB p65 immunoreactivity increased under hypoxia in both cortex and hippocampus and was reduced in the treated groups, with the most pronounced reduction in the Hypoxia+CNPs/Orientin group (Figs. 14, 15, 16). This protein-level finding is also consistent with the attenuation of inflammatory signaling observed in the cytokine and RT-PCR analyses.

The obtained data suggest that hypoxic neuronal injury evolves through interconnected feed-forward and feedback loops, in which HIF-1α activation [46] is accompanied by increased iNOS expression and oxidative stress, which may further amplifies NF-κB/TNF-α signaling [47] and ultimately converge on Caspase-3- linked apoptosis [29, 30]. This integrated cascade provides a mechanistic framework supporting multi-target neuroprotective strategies, including flavonoid-based nanoformulations [35].

This multi-level parallelism concretely confirms the neuroprotective efficacy of combination therapy at the histological level. Indeed, several experimental models have reported that delivering flavonoids in nanoparticle formulations enhances bioavailability and provides sustained histological protection [36, 48]. To the best of our knowledge, this study provides novel experimental evidence that Orientin-loaded CNPs confer concurrent neuronal and vascular protection in this in vivo hypoxia rat model**,** supported by concordant biochemical, molecular, and histopathological findings [30, 36].

While our findings corroborate prior work, our data further indicate that combining Orientin with CNPs can mitigate pharmacokinetic limitations in this in vivo hypoxia model; however, some studies have reported that flavonoids alone exhibit stronger antioxidant effects. This discrepancy is attributable to differences in experimental models and pharmacokinetic conditions. Xu and colleagues administered

luteolin, and Alqahtani and colleagues administered quercetin directly; thus, limiting factors such as bioavailability and the blood–brain barrier were eliminated [49]. In contrast, in our in vivo hypoxia model, Orientin was administered systemically; therefore, pharmacokinetic limitations, such as solubility, metabolic degradation, and tissue penetration, may have limited its efficacy alone. Therefore, our findings suggest that combining Orientin with CNPs may help mitigate these pharmacokinetic limitations and produce a more pronounced antioxidant effect.

Limitations

The present study has several limitations. First, only male rats were used with a modest sample size ($n = 6$ per group), which may limit generalizability and the statistical power to detect small effect sizes. Second, the hypoxia exposure period was relatively short (8 h/day for 7 days); therefore, longer follow-up studies are required to determine the durability of the observed neuroprotective effects. In addition, functional and behavioral assessments were not performed, and thus biochemical, molecular, and histopathological improvements cannot be directly linked to neurobehavioral recovery. Furthermore, pharmacokinetic and biodistribution parameters, including brain orientin levels, release kinetics, and blood–brain barrier penetration, were not evaluated; consequently, the enhanced efficacy of orientin-loaded CNPs is interpreted as being consistent with improved delivery rather than directly confirmed. Although we assessed total NF-κB p65 expression and NF-κB-regulated downstream cytokines (e.g., TNF-α and IL-1β), phosphorylated NF-κB p65 was not quantified; therefore, NF-κB pathway activation could not be directly confirmed. Given the large number of biochemical, molecular, and histopathological endpoints included in the study, effect size analyses were not reported for all comparisons. Instead, treatment effects were interpreted according to the predefined statistical analysis plan and the overall biological consistency of the findings across the different levels of analysis.

Author Contributions Author contributions İ.T. Ç.A. E.B. A.K. A.Y. V.G. G.B. E.E G.Ö.: experiment design, experiment application, samples collection. V.G A.K.: serum markers and tissue antioxidant estimation, data curation and analysis, final reviewing. E.E.: histopathological investigation. All authors contributed to the writing and editing, and they read and approved the final manuscript. The authors declare that all data were generated in-house and that no paper mill was used.

Funding This work was not supported by any institution.

Data Availability The authors confirm that the data and materials supporting the findings of this study are available within the article.

Declarations

Ethics Approval The study was designed and conducted according to ethical norms approved by the Kafkas University Animal Experiments Local Ethics Committee (Kars, Turkey) (KAÜ-HADYEK/2025/245).

Consent to Participate All authors voluntarily participated in this research study.

Consent for Publication All authors have consent for the publication of the manuscript.

Conflict of interest The authors declare no competing interests.

References

1. Coimbra-Costa D, Alva N, Duran M, Carbonell T, Rama R (2017) Oxidative stress and apoptosis after acute respiratory hypoxia and reoxygenation in rat brain. Redox Biol 12:216–225
2. Han Y, Ding L, Cheng X, Zhao M, Zhao T, Guo L et al (2020) Hypoxia augments cerebral inflammation in a dextran sulfate sodium-induced colitis mouse model. Front Cell Neurosci 14:611764
3. He Q, Ma Y, Liu J, Zhang D, Ren J, Zhao R et al (2021) Biological functions and regulatory mechanisms of hypoxia-inducible factor-1α in ischemic stroke. Front Immunol 12:801985
4. Gabryelska A, Sochal M (2022) Evaluation of HIF-1 involvement in the BDNF and proBDNF signaling pathways among obstructive sleep apnea patients. Int J Mol Sci 23(23):14876
5. Lu DY, Liou HC, Tang CH, Fu WM (2006) Hypoxia-induced iNOS expression in microglia is regulated by the PI3-kinase/Akt/mTOR signaling pathway and activation of hypoxia inducible factor-1α. Biochem Pharmacol 72(8):992–1000
6. Agafonova A, Cosentino A, Musso N, Prinzi C, Russo C, Pellitteri R et al (2025) Hypoxia-induced inflammation in in vitro model of human blood–brain barrier: modulatory effects of the olfactory ensheathing cell-conditioned medium. Mol Neurobiol 62:4008–4022
7. Bellavite P (2023) Neuroprotective potentials of flavonoids: experimental studies and mechanisms of action. Antioxidants (Basel) 12(2):280
8. Hasan S, Khatri N, Rahman ZN, Menezes AA, Martini J, Shehjar F et al (2023) Neuroprotective potential of flavonoids in brain disorders. Brain Sci 13(9):1258
9. Wang X, An F, Wang S, An Z, Wang S (2017) Orientin attenuates cerebral ischemia/reperfusion injury in rat model through the AQP-4 and TLR4/NF-κB/TNF-α signaling pathway. J Stroke Cerebrovasc Dis 26(10):2199–2214
10. Fahmy MI, Sadek MA, Abdou K, El-Dessouki AM, El-Shiekh RA, Khalaf SS (2025) Orientin: a comprehensive review of a promising bioactive flavonoid. Inflammopharmacology 33(4):1713–1728
11. Caprifico AE, Foot PJS, Polycarpou E, Calabrese G (2020) Overcoming the blood-brain barrier: functionalised chitosan nanocarriers. Pharmaceutics 12(11):1013
12. Divya K, Jisha MS (2018) Chitosan nanoparticles preparation and applications. Environ Chem Lett 16(1):101–112
13. Qi L, Xu Z, Jiang X, Hu C, Zou X (2004) Preparation and antibacterial activity of chitosan nanoparticles. Carbohydr Res 339(16):2693–2700
14. Calvo P, Remuñán-López C, Vila-Jato JL, Alonso MJ (1997) Chitosan and chitosan/ethylene oxide-propylene oxide block

copolymer nanoparticles as novel carriers for proteins and vaccines. J Appl Polym Sci 63(1):125–132
15. Agnihotri SA, Mallikarjuna NN, Aminabhavi TM (2004) Recent advances on chitosan-based micro- and nanoparticles in drug delivery. J Control Release 100(1):5–28
16. Xu XM, Yao D, Cai XD, Ding C, Lin QD, Wang LX et al (2015) Effect of chronic continual- and intermittent hypoxia-induced systemic inflammation on the cardiovascular system in rats. Sleep Breath 19(2):677–684
17. Stolk JA, Olsen JI, Reeves PM, Chen M, Perry C, Alderman DW et al (1989) In vivo [31P]NMR studies on the influence of age on rat brain hypoxia. Brain Res 482(1):1–11
18. Thangaraj K, Natesan K, Palani M, Vaiyapuri M (2018) Orientin, a flavanoid, mitigates 1, 2 dimethylhydrazine-induced colorectal lesions in Wistar rats fed a high-fat diet. Toxicol Rep 1(5):977–987
19. Şehirli AÖ, Sayıner S, Bilginaylar K, Özkayalar H, Aykaç A (2024) Does chitosan introduce protection against methotrexate-induced hepatorenal injury in rats? Clin Exp Health Sci 14(1):39–44
20. Passmore MR, Byrne L, Obonyo NG, See Hoe LE, Boon AC, Diab SD et al (2018) Inflammation and lung injury in an ovine model of fluid resuscitated endotoxemic shock. Respir Res 19:1–10
21. Erbaş E, Celep NA, Tekiner D, Genç A, Gedikli S (2024) Assessment of toxicological effects of favipiravir (T-705) on the lung tissue of rats: an experimental study. J Biochem Mol Toxicol 38(1):e23536
22. Hübner RH, Gitter W, El Mokhtari NE, Mathiak M, Both M, Bolte H et al (2008) Standardized quantification of pulmonary fibrosis in histological samples. Biotechniques 44(4):507–517
23. Shushanyan R, Grigoryan A, Abgaryan T, Karapetyan A (2023) Histological and cytochemical analysis of the brain under conditions of hypobaric hypoxia-induced oxygen deficiency in albino rats. Acta Histochem 125(8):152114
24. Soliman H, Rawal B, Fulp J, Lee JH, Lopez A, Bui MM et al (2013) Analysis of indoleamine 2,3-dioxygenase (IDO1) expression in breast cancer tissue by immunohistochemistry. Cancer Immunol Immunother 62:829–837
25. Ishii Y, Sasaki T, Serikawa M, Minami T, Okazaki A, Yukutake M et al (2013) Elevated expression of cyclooxygenase-2 and microsomal prostaglandin E synthase-1 in primary sclerosing cholangitis: implications for cholangiocarcinogenesis. Int J Oncol 43(4):1073–1079
26. Bernkop-Schnürch A, Dünnhaupt S (2012) Chitosan-based drug delivery systems. Eur J Pharm Biopharm 81(3):463–469
27. Dash M, Chiellini F, Ottenbrite RM, Chiellini E (2011) Chitosan—a versatile semi-synthetic polymer in biomedical applications. Prog Polym Sci 36(8):981–1014
28. Keawchaoon L, Yoksan R (2011) Preparation, characterization and in vitro release study of carvacrol-loaded chitosan nanoparticles. Carbohydr Polym 83(4):1620–1628
29. Merelli A, Repetto M, Lazarowski A, Auzmendi J (2021) Hypoxia, oxidative stress, and inflammation: three faces of neurodegenerative diseases. J Alzheimers Dis 82(s1):S109–S126
30. Amine BE, Fournier J, Minoves M, Baillieul S, Roche F, Perek N et al (2024) Cerebral oxidative stress, inflammation and apoptosis induced by intermittent hypoxia: a systematic review and meta-analysis of rodent data. Eur Respir Rev 33(174):240162
31. Reay SL, Ferreira AM, Hilkens CMU, Novakovic K (2025) The paradoxical immunomodulatory effects of chitosan in biomedicine. Polymers (Basel) 17(1):19
32. Valades-Aguilar BA, Rivera-González TI, Rangel-López R, Luna-Barcenas G, Franco-Molina MÁ, Rodriguez-Padilla C et al (2024) Influence of chitosan purification on the immunomodulator potential of chitosan nanoparticles on human monocytes. Polymers (Basel) 16(23):3390
33. Wang Z, Yan Y, Zhang Z, Li C, Mei L, Hou R et al (2024) Effect of chitosan and its water-soluble derivatives on antioxidant activity. Polymers 16(7):867
34. Chen G, Wang X, Jin Z, Hu GB, Yu QH, Jiang HY (2024) HIF-1α knockdown attenuates inflammation and oxidative stress in ischemic stroke male rats via CXCR4/NF-κB pathway. Brain Behav 14(9):e70039
35. Prasanna P, Upadhyay A (2021) Flavonoid-based nanomedicines in Alzheimer's disease therapeutics: promises made, a long way to go. ACS Pharmacol Transl Sci 4(1):74–95
36. Abdi Syahputra R, Dalimunthe A, Utari ZD, Halim P, Sukarno MA, Zainalabidin S et al (2024) Nanotechnology and flavonoids: current research and future perspectives on cardiovascular health. J Funct Foods 120:106355
37. Faiyaz Khan M, Ahmad N, Alkholifi FK, Ullah Z, Saifuddin Khalid M, Akhtar S et al (2024) Preparation of novel S-allyl cysteine chitosan based nanoparticles for use in ischemic brain treatment. RSC Adv 14(1):160–180
38. Li L, Jiang W, Yu B, Liang H, Mao S, Hu X et al (2023) Quercetin improves cerebral ischemia/reperfusion injury by promoting microglia/macrophages M2 polarization via regulating PI3K/Akt/NF-κB signaling pathway. Biomed Pharmacother 168:115653
39. Chávez JC, Agani F, Pichiule P, LaManna JC (2000) Expression of hypoxia-inducible factor-1α in the brain of rats during chronic hypoxia. J Appl Physiol 89(5):1937–1942
40. Kiuchi M, Uno T, Hasegawa T, Koyama K, Horiuchi M (2024) Influence of short-term hypoxic exposure on spatial learning and memory function and brain-derived neurotrophic factor in rats—a practical implication to human's lost way. Front Behav Neurosci 18:1330596
41. Stefanache A, Lungu II, Anton N, Damir D, Gutu C, Olaru I et al (2025) Chitosan nanoparticle-based drug delivery systems: advances, challenges, and future perspectives. Polymers (Basel) 17(11):1453
42. Huang B, Liu J, Fu S, Zhang Y, Li Y, He D et al (2020) α-Cyperone attenuates H2O2-induced oxidative stress and apoptosis in SH-SY5Y cells via activation of Nrf2. Front Pharmacol 11:281
43. Khallaf WAI, Sharata EE, Attya ME, Rofaeil RR, Khalaf MM, Hemeida RAM et al (2025) Buspirone ameliorates premature ovarian insufficiency evoked by cyclophosphamide in female rats; attention to AMPK/Nrf2/HO-1, α-Klotho/NLRP3/Caspase-1, and Caspase-3-mediated apoptosis interplay. Toxicol Appl Pharmacol 500:117373
44. Lu G, Rili G, Shuang M (2025) Impact of hypoxia on the hippocampus: a review. Medicine 104(12):e41479
45. Choi YK (2024) Detrimental roles of hypoxia-inducible factor-1α in severe hypoxic brain diseases. Int J Mol Sci 25(8):4465
46. Lv R, Zhou W, Duan M, Ge Y, Zhong T (2008) Ultrastructural changes, nuclear factor-κB activation, and tumor necrosis factor-α expression in brain after acute normovolemic hemodilution and controlled hypotension in rats. Croat Med J 49(1):22–31
47. Li Z, Zhang J, Zhang X, Jin Q, Zheng X, Mo L et al (2025) Oxygen metabolism abnormalities and high-altitude cerebral edema. Front Immunol 16:1555910
48. Xu J, Wang H, Ding K, Zhang L, Wang C, Li T et al (2014) Luteolin provides neuroprotection in models of traumatic brain injury via the Nrf2–ARE pathway. Free Radic Biol Med 71:186–195
49. Wróbel-Biedrawa D, Grabowska K, Galanty A, Sobolewska D, Podolak I (2022) A flavonoid on the brain: quercetin as a

potential therapeutic agent in central nervous system disorders. Life 12(4):591

Publisher's Note Springer Nature remains neutral with regard to jurisdictional claims in published maps and institutional affiliations.

Springer Nature or its licensor (e.g. a society or other partner) holds exclusive rights to this article under a publishing agreement with the author(s) or other rightsholder(s); author self-archiving of the accepted manuscript version of this article is solely governed by the terms of such publishing agreement and applicable law.